Structure and Chemistry of Zircon and Zircon-Group Minerals

Robert J. Finch

Argonne National Laboratory
9700 South Cass Avenue
Argonne, Illinois 60439

John M. Hanchar

Department of Earth and Environmental Sciences
The George Washington University
Washington, D.C. 20006

INTRODUCTION

Zircon ($ZrSiO_4$) is a common accessory mineral in nature, occurring in a wide variety of sedimentary, igneous, and metamorphic rocks. Known to incorporate an assortment of minor and trace elements, zircon has the ability to retain substantial chemical and isotopic information, leading to its use in a wide range of geochemical investigations, including studies on the evolution of Earth's crust and mantle (e.g., Hanchar et al. 1994, Bowring 1995, Vervoort et al. 1996, Hoskin and Schaltegger, this volume; Valley, this volume) as well as age dating (e.g., Gibson and Ireland 1995, Bowring et al. 1998, Solar et al. 1998, Bowring and Schmitz, this volume; Ireland and Williams, this volume; Parrish et al., this volume). The physical and chemical durability of zircon is a major factor in it being the mineral by which many of Earth's oldest known rocks have been dated (Bowring et al. 1989, Maas et al. 1992, Buick et al. 1995, Bowring and Williams 1999, Wilde et al. 2001) and is also an important factor in zircon being proposed as a candidate waste form for the geologic disposal of excess plutonium from dismantled nuclear weapons (Ewing and Lutze 1997, Ewing 1999, Burakov et al. 2002, Burakov et al. 2003, Ewing et al., this volume).

The chemical and physical properties of zircon and its ability to incorporate and retain trace elements are largely determined by its crystal structure. The zircon structure is adopted by numerous minerals and synthetic compounds with the general formula ATO_4, in which high field-strength *T*-site cations occupy isolated tetrahedra, and *A*-site cations occupy larger eight-coordinated structural sites. Zircon-type compounds share many physical properties, as well as displaying variable degrees of solid solution among end members. Because many zircon-group minerals commonly contain radioactive U and Th, natural crystals commonly suffer substantial radiation damage, and most precise structure determinations are based on studies of synthetic analogues (e.g., Taylor and Ewing 1978, Ni et al. 1995, Finch et al. 2001a, Boatner 2002). We rely to a large extent on results from structural studies of synthetic analogues of zircon and zircon-group minerals in this review.

In the sections that follow, we provide an overview of the crystalline structure of zircon, followed by brief discussions of naturally occurring ATO_4 compounds that are isostructural with zircon; these are the zircon-group minerals. We also compare the zircon structure with structures of several related compounds, including those of scheelite and monazite, because of the importance that these structures have in understanding phase relationships among zircon-group minerals and their polymorphs. We conclude with a discussion of some effects that changes in pressure, temperature and composition can have on the structure of zircon. Throughout the text, we use the acronym REE (rare-earth elements) to include Sc, Y and the lanthanide elements (La through Lu).

1529-6466/03/0053-0001$05.00

STRUCTURE OF ZIRCON

Zircon is an orthosilicate in which isolated SiO_4 tetrahedra share corners and edges with ZrO_8 dodecahedra. The ZrO_8 dodecahedra share edges with each other to form chains parallel to <100> (Fig. 1) such that each ZrO_8 polyhedron shares edges with four adjacent ZrO_8 polyhedra, two in each of the crystallographically equivalent directions [100] and [010]. These <100> chains of ZrO_8 polyhedra are cross linked by sharing corners with SiO_4 tetrahedra (perpendicular to the page in (Fig. 1). The *Si* and *Zr* polyhedra also form an edge-connected chain of alternating ZrO_8 and SiO_4 polyhedra parallel to [001] (Fig. 1), between which lie unoccupied channels, also parallel to [001] (Fig. 2). The [001] edge-connected chains of *Zr* and *Si* polyhedra comprise an especially strongly connected feature in the structure, as manifested in many physical properties of zircon, including its prismatic habit, {110} cleavage, high birefringence (Speer 1982a and references therein), anisotropic thermal expansion (Bayer 1972, Subbarao et al. 1990) and compression (Hazen and Finger 1979, Smyth et al. 2000, van Westrenen et al. 2003a).

Zircon is tetragonal and crystallizes in space group $I4_1/amd$. Both cations (Zr^{4+} and Si^{4+}) occupy special positions with site symmetry $\bar{4}2m$. The O atom occupies a site with symmetry *m*: the *y* and *z* coordinates of the O atom are the only refineable atomic-site parameters in the zircon structure ($y = 0.066$, $z = 0.195$; Hazen and Finger 1979, Finch et al. 2001a, also see Speer 1982a). Each O atom is bonded to one Si atom at 1.62 Å and two Zr atoms at 2.13 and 2.27 Å, so that each Zr atom is bonded to four O atoms at 2.13 Å and another four at 2.27 Å (Hazen and Finger 1979, Finch et al. 2001a).

Cation polyhedra

The SiO_4 tetrahedron in zircon is a tetragonal disphenoid (symmetry $\bar{4}2m$) elongated parallel to [001]. This distortion of the regular SiO_4 tetrahedron has been attributed to repulsion between the Zr^{4+} and Si^{4+} cations, whose polyhedra share a common edge (Speer 1982a). The two O-Si-O angles in the SiO_4 group are approximately 97° and 116° (Hazen and Finger 1979, Finch et al. 2001a). The O-O distance along the polyhedral edge shared with the ZrO_8 polyhedron is 2.43 Å (opposite the smaller O-Si-O angle) and 2.75 Å along the unshared edge (opposite the larger O-Si-O angle).

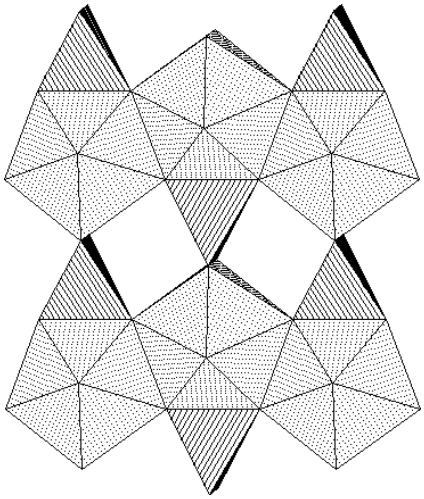

Figure 1. Zircon structure projected on (100); *c* axis is vertical, *b* (a_2) axis is horizontal. ZrO_8 dodecahedra are shaded light gray; SiO_4 tetrahedra are striped.

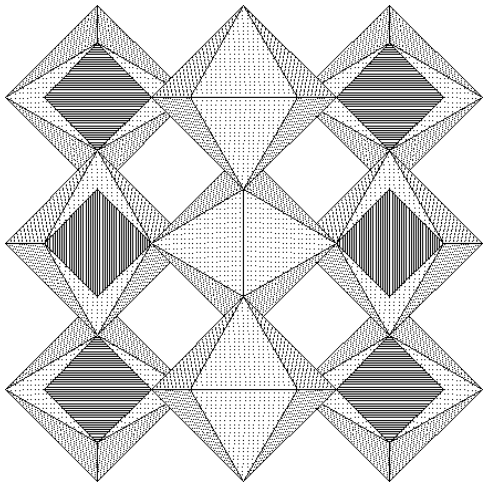

Figure 2. Zircon structure projected on (001), showing view down the [001] channels (unshaded). Shading as for Figure 1.

The Zr atom is coordinated by eight O atoms that define a triangular dodecahedron with symmetry $\bar{4}2m$. The ZrO_8 dodecahedron in zircon can be described as two interpenetrating ZrO_4 tetrahedra (Nyman et al. 1984): one elongated along [001], which we will call ZrO_4^e, the other compressed, ZrO_4^c (nomenclature after Ríos et al. 2000) (Fig. 3). (Note that if both tetrahedra were undistorted, the polyhedron that would result from their interpenetration is a cube). As noted above, there are four long and four short Zr-O distances in zircon. The four long Zr-O bond distances are associated with the elongated ZrO_4^e tetrahedron, and the four short Zr-O bond distances are associated with the ZrO_4^c tetrahedron. Using this description, one can visualize the chains of edge-sharing ZrO_8 and SiO_4 polyhedra as isolated chains of edge-sharing SiO_4 and ZrO_4^e tetrahedra, both being tetragonal disphenoids elongated along [001] (Fig. 4). The compressed ZrO_4^e tetrahedra are then seen to share their four corners with SiO_4 tetrahedra, forming a tetrahedral array that Nyman et al. (1984) describe as a "C9-type" superstructure (as occurs in "ideal" high cristobalite). In this context, the zircon structure is built of two unconnected interpenetrating C9-type arrays of corner-sharing SiO_4 and ZrO_4^c tetrahedra (Fig. 5).

Interstitial sites

The structure of zircon is relatively open, with small voids between the SiO_4 and ZrO_8 polyhedra (Fig. 1) and open channels parallel to [001] (Fig. 2). Such structural voids are potential interstitial sites that could incorporate impurities, provided that such sites can accommodate interstitial ions without excessive structural strain. Interstices have been proposed as potential sites for many impurity elements reported from zircon analyses (Speer 1982a). Although most detailed studies of elemental substitution in zircon find that impurity cations can usually be accounted for by substitutions at either the *Zr* or *Si* sites, both natural and synthetic zircon crystals can display non-stoichiometry (e.g., Hinton and Upton 1991, Hoskin et al. 2000, Hanchar et al. 2001a). Finch et al. (2001a) suggested that interstitial sites may incorporate low levels of impurity cations in synthetic zircon crystals. Although present at concentrations below detection by many conventional analytical methods (a few ppm to several tens of ppm), interstitial cations can have a significant impact on charge-balancing heterovalent substitutions on *Zr* and *Si* sites. The possible role of interstitial sites is a potentially fruitful area of research on zircon crystal chemistry.

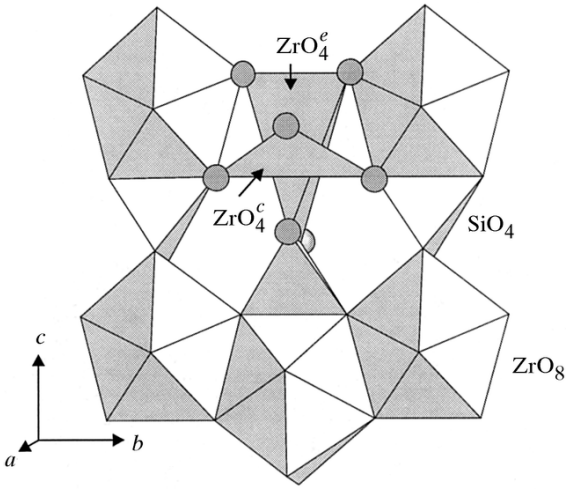

Figure 3. View of zircon structure projected on (100) (same orientation as Fig. 1) illustrating extended (ZrO_4^e) and compressed (ZrO_4^c) tetrahedra (from Ríos et al. 2000).

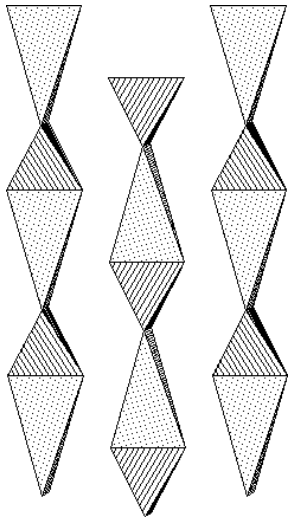

Figure 4. Zircon structure projected on (100), illustrating [001] chains of edge-sharing tetrahedra: ZrO_4^e (light gray stippled) and SiO_4 (darker gray striped); *c* axis is vertical and *b* axis horizontal.

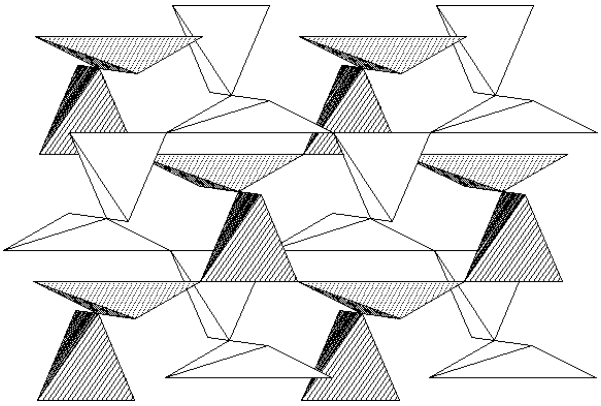

Figure 5. Interpenetrating C9-type arrays of SiO_4 and ZrO_4[c] tetrahedra in zircon. View is approximately down [100], with *c* axis vertical and *b* axis horizontal. Different shadings are to illustrate the two C9-type tetrahedral arrays.

One interstitial site is a distorted octahedron that shares faces with two ZrO_8 polyhedra and two SiO_4 tetrahedra (Fig. 1) and lies approximately 1.87 Å from two *O* sites and 2.08 Å from four *O* sites. The proximity of two Si^{4+} ions (each at 1.84 Å) across a shared polyhedral face makes this an unlikely site for high field-strength cation impurities. The second interstice is a four-coordinated site that lies within the channels parallel to [001] (Fig. 2). It is adjacent to the distorted octahedral interstice and shares a face with it. This interstice is 1.84 Å from four adjacent *O* sites and shares one face with a neighboring ZrO_8 polyhedron (Fig. 6). Low levels of small, high-field-strength ions may be compatible with this site.

Few studies have examined the energetics of impurity substitutions in the zircon structure, including the potential role of interstitial sites. Williford et al. (2000) calculated the energetics of defects in Pu-doped zircons and found that an O vacancy may be stabilized by two Pu^{3+} substitutions at nearby *Zr* sites. Crocombette (1999) calculated the energetics of point defects in zircon (pure $ZrSiO_4$), including Zr, Si and O interstitials and vacancies, and found that interstitial Zr and Si atoms tend to occupy interstices within the open channels along [001], whereas O interstitials tend to occur as one of a dumbbell-shaped pair of O atoms coordinated to a common Si (making a five-coordinated *Si* site). The results of the study by Crocombette (1999) indicate that, with the exception of O interstitials, formation energies for all point defects (interstitials and vacancies) ensure that the equilibrium thermal concentration of point defects in pure zircon is negligible. Furthermore, because the activation energy for O diffusion is less than that required for O-vacancy formation (Williford et al. 1999), O vacancies are unlikely to persist in zircon, especially over geologic time spans.

ZIRCON-GROUP MINERALS

Several minerals and numerous synthetic ATO_4 compounds are isostructural with zircon (Table 1). Classified according to the tetrahedrally coordinated *T*-site cations, zircon-group minerals include silicates, phosphates, vanadates, borates, an arsenate, and a chromate. Dodecahedral *A*-site cations range from low field-strength cations such as Ca^{2+} to high field-strength cations such as Ta^{5+} and Nb^{5+}. With the notable exception of $ZrGeO_4$ (with $c/a = 0.936$), compounds having the zircon structure are characterized by axial ratios (c/a) between 0.869 (for chromatite, $CaCrO_4$) and 0.908 (for hafnon, $HfSiO_4$), a rather narrow range given the variety of *A*- and *T*-site cations compatible with the zircon structure (Table 1). Axial ratios depend in part on the degree of repulsion between adjacent *A*-site cations and between *A*- and *T*-site cations, due to the fact that the *A* site (*Zr* dodecahedron) shares edges with both *A*- and *T*-site polyhedra (Fig. 1). Strong repulsion

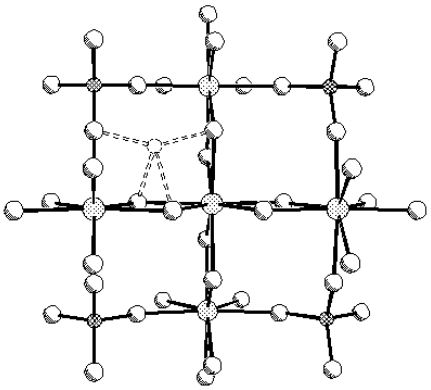

Figure 6. Zircon structure viewed approximately down [001] illustrating the four-coordinated interstitial site (same orientation as for Fig. 2).

Table 1. Zircon-group minerals and selected synthetic zircon-type compounds*

Name	Formula	**a**	**c**	V	c/a	density	Ref.
Zircon	$ZrSiO_4$	6.607	5.9835	261.2	0.906	4.66	[1]
Hafnon	$HfSiO_4$	6.577	5.969	258.2	0.908	6.98	[2]
Thorite	$ThSiO_4$	7.1335	6.3205	321.6	0.886	6.70	[3]
Coffinite	$USiO_4$	6.979	6.253	304.6	0.896	6.90	[4]
Xenotime	YPO_4	6.895	6.027	286.5	0.874	4.28	[5]
Xenotime-(Yb)	$YbPO_4$	6.438	6.400	276.5	0.874	6.44	[5]
Pretulite	$ScPO_4$	6.589	5.806	252.1	0.881	3.71	[6]
Chromatite	$CaCrO_4$	7.242	6.290	329.9	0.869	3.14	[7]
Behierite	$(Ta,Nb)BO_4$	6.206	5.472	210.8	0.882	7.37	[8]
Schiavinatoite	$(Nb,Ta)BO_4$	6.219	5.487	212.2	0.882	6.57	[9]
Wakefieldite-(Y)	YVO_4	7.118	6.289	318.7	0.884	4.25	[10,11]
Wakefieldite-(Ce)	$(Ce,Pb)VO_4$	7.35	6.56	352.8	0.893	5.30	[12]
Wakefieldite-(Ce)	$CeVO_4$	7.354	6.488	350.9	0.882	4.83	[13]
Dreyerite	$BiVO_4$	7.303	6.458	344.4	0.884	6.25	[14]
	$CeVO_4$	7.400	6.497	355.8	0.878	4.76	[11]
	$LuVO_4$	7.025	6.234	307.7	0.887	6.25	[11]
	$ScVO_4$	6.780	6.135	282.0	0.905	3.76	[11]
Chernovite-(Y)	$YAsO_4$	7.044	6.248	310.0	0.887	4.85	[15]
	$SmAsO_4$	7.20	6.40	331.8	0.890	5.77	[16]
	$LuAsO_4$	6.949	6.227	300.7	0.896	6.94	[17]
	$PrCrO_4$	7.344	6.428	346.7	0.875	4.92	[18]
	$LuCrO_4$	7.027	6.200	306.1	0.882	6.31	[18]
	$ThGeO_4$	7.230	6.539	341.8	0.904	7.16	[19]
	$ZrGeO_4$	6.694	6.265	280.7	0.936	5.43	[20]

* *Notes*: unit-cell parameters (***a***,***c***) in Å; unit-cell volume in $Å^3$; density in g cm^{-3}.
References: [1] Finch et al. (2001); [2] Speer and Cooper (1982); [3] Taylor and Ewing (1978); [4] Fuchs and Gebert (1958); [5] Ni et al. (1995); [6] Bernard (1998); [7] Weber and Range (1996); [8] Mrose and Rose (1961); [9] Demartin et al. (2001); [10] Miles et al. (1971); [11] Chakoumakos et al. (1994); [12] Deliens and Piret (1977); [13] Baudracco-Gritti et al. (1987); [14] Dreyer and Tillmanns (1981); [15] Goldin et al. (1967); [16] Durif and Forrat (1957); [17] Lomüller et al. (1973); [18] Buisson et al. (1964); [19] Ennaciri et al. (1986); [20] Hirano et al. (2002a).

between *A*- and *T*-site cations tends to increase *c*/*a* (lengthening the *c* axis), whereas strong repulsion between adjacent *A*-site cations tends to decrease *c*/*a* (longer *a*). Although readily identified from their similar X-ray powder diffraction patterns as possessing the zircon structure, complete structural details are still unknown for many zircon-group minerals.

The zircon structure shares structural similarities with the minerals scheelite ($CaWO_4$), monazite ($CePO_4$), rutile (TiO_2), garnet ($X_3Y_2T_3O_{12}$), and anhydrite ($CaSO_4$), and some of these similarities are discussed in the section on related structures below. Reidite, the naturally occurring high-pressure $ZrSiO_4$ polymorph (Glass et al. 2002a,b), is isostructural with scheelite; whereas huttonite, the high-pressure and high-temperature polymorph of $ThSiO_4$, is isostructural with monazite. The fact that the high-pressure polymorphs of the isostructural minerals zircon and thorite are not themselves isostructural attests to the importance of *A*- and *T*-site cations in determining polymorphic transitions. At room temperature and pressure, silicates, vanadates, and chromates crystallize with the zircon structure, whereas germanates, molybdates, tungstates,

periodates, and pertechnetates crystallize with the scheelite structure. Phosphates and arsenates crystallize with the zircon structure for middle and heavy lanthanides, Y and Sc, and with the monazite structure for the larger light lanthanides. $LaVO_4$ is the only orthovanadate with the monazite structure; all other REE orthovanadates possess the zircon structure at room temperature and pressure.

Crystal structure is determined primarily by the sizes of ions that make up a crystal (Carron et al. 1958, Fukunaga and Yamaoka 1979). A plot showing the sum of *A* and *T* cation radii versus the ratio of ionic radii $^{[VIII]}A/^{[IV]}T$ for ATO_4 compounds known to form zircon-, scheelite-, or monazite-type structures illustrates the importance of *A* and *T* cations in determining ATO_4 structure type (Fig. 7: $^{[IV]}T = B^{3+}$, Si^{4+}, Ge^{4+}, P^{5+}, V^{5+}, As^{5+}, Cr^{5+}, Cr^{6+}, Mo^{6+}, W^{6+}, S^{6+}, Tc^{7+}, I^{7+}). Zircon- and monazite-type structures tend to be adopted by ATO_4 compounds with *T*-site cations smaller than Ge^{4+} (0.390 Å) or Tc^{7+} (0.37 Å) and larger than S^{6+} (0.12 Å), with the exception of $(Ta,Nb)BO_4$, which is isostructural with zircon (effective ionic radii are from Shannon 1976). There is less apparent dependence on the radius of the *A*-site cation, although the zircon structure is adopted by compounds with the smallest *A*-site cations compatible with a given *T*-site cation. The scheelite structure is adopted by compounds with the largest *T*-site cations (Ge^{4+}, Mo^{6+}, W^{6+}, Tc^{7+}, I^{7+}) and all but the smallest *A*-site cations (which tend to form ATO_4 compounds with the wolframite structure); however, germanates form zircon-type structures at elevated temperatures (Bayer 1972). The monazite structure is adopted by ATO_4 compounds with *A*-site cations comparable to, but slightly larger than *A*-site cations in zircon-type structures.

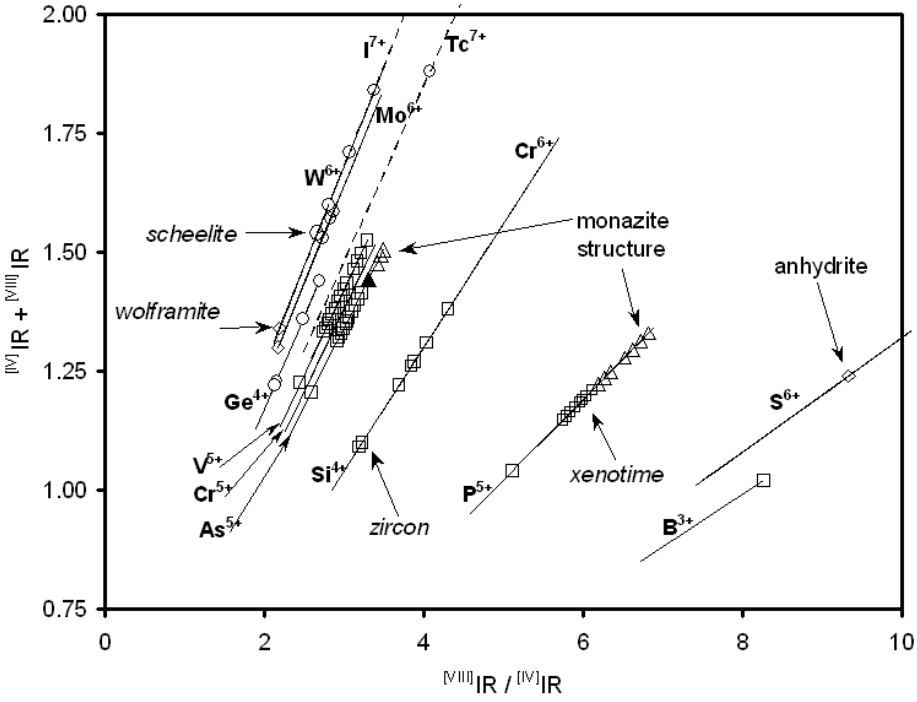

Figure 7. Plot showing sums of *A* and *T* cation radii ($^{[VIII]}A + {}^{[IV]}T$) versus their radius ratios ($^{[VIII]}A/^{[IV]}T$) for ATO_4 compounds known to adopt structure types discussed in the text. Lines indicate the range of values compatible with each *T*-site cation, and symbols indicate selected known structures. Squares designate zircon-type compounds; triangles are monazite-type compounds; circles correspond to scheelite-type compounds (diamonds are other structures). Structure types are indicated for room-temperature polymorphs where known (shaded circle is $NaIO_4$; filled triangle is $NdAsO_4$). Effective ionic radii from Shannon (1976).

Silicates

The structure of hafnon ($HfSiO_4$) is identical to that of zircon in virtually all details except small differences in bond lengths and angles (Speer and Cooper 1982). The ionic radius of $^{[VIII]}Hf^{4+}$ (0.83 Å) is only slightly smaller than that of $^{[VIII]}Zr^{4+}$ (0.84 Å), and the unit-cell dimensions of hafnon are correspondingly similar to those of zircon, with pure $HfSiO_4$ having smaller volume (Table 1). In fact, the similar chemistries of Zr and Hf long delayed discovery of Hf, which was first found in zircon in 1923 by D. Coster and G.C. von Hevesey. The estimated crustal abundance of Zr and Hf corresponds to an atomic ratio Zr:Hf approximately equal to 70:1 (Rudnick and Fountain 1995, Taylor and McLennan 1995, Wedepohl 1995); this is the atomic ratio Zr:Hf in zircon with 1.3 wt % Hf (1.6 wt % HfO_2). Zircon crystals typically contain less than about 3 wt % Hf, with concentrations ranging between 0.5 and 7 wt % Hf (Hoskin and Schaltegger, this volume); however, complete solid solution between end-member compositions has been demonstrated (Ramakrishnan et al. 1969, Hoskin and Rodgers 1996).

Actinide silicates

There are three naturally occurring ATO_4 actinide silicates, two of which are isostructural with zircon: coffinite ($USiO_4$) and thorite ($ThSiO_4$). Thorite is one of two naturally occurring polymorphs of $ThSiO_4$. The structures of thorite and zircon are completely analogous. The SiO_4 tetrahedron in thorite is essentially identical to that in zircon, with Si-O distances of 1.63 Å (Taylor and Ewing 1978). The two Th-O distances at 2.37 Å and 2.47 Å, are 11% and 9% longer than the corresponding Zr-O distances in zircon (2.13 and 2.27 Å), reflecting the larger radius of the Th^{4+} ion (1.05 Å). Thorite is the polymorph stable at room temperature and pressure, transforming to huttonite, the denser lower-symmetry polymorph, at elevated pressure and temperature (Dachille and Roy 1964, Finch et al. 1964). Huttonite is monoclinic and isostructural with monazite (Taylor and Ewing 1978), the structure of which is described in more detail in the section on related structures.

Coffinite ($USiO_4$) forms as an alteration product of uraninite (UO_2) under reducing conditions and has been identified in many diverse U deposits (Janeczek 1991, Janeczek and Ewing 1992, Fayek and Kyser 1997, Fayek et al. 1997). Coffinite occurs in nature as microscopic intergrowths that are unsuitable for structure determination by conventional X-ray diffraction methods, and hydrothermal syntheses produce only fine-grained powders (Hoekstra and Fuchs 1956). The isostructural relationship between zircon and coffinite was established by a detailed X-ray powder diffraction study of synthetic coffinite (Fuchs and Gebert 1958), and lattice parameters of coffinite and thorite suggest that structural details for those two minerals are similar (Table 1). No single-crystal structure data are available for coffinite, nor are we aware of any reported neutron powder structure refinements of coffinite, although such a study would be valuable.

Although coffinite is isostructural with thorite, the degree of solid solution between the two phases is uncertain, with conflicting reports in the literature. Fuchs and Gebert (1958) reportedly synthesized the complete series $(U,Th)SiO_4$, but Mumpton and Roy (1961) found the limit on U substitution to be about 30 mol % $USiO_4$. Variations in synthesis methods and temperatures may help explain the differences. Natural coffinite may contain substantial amounts of REE and P, suggesting some solid solution with xenotime, YPO_4 (Hansley and Fitzpatrick 1989, Janeczek and Ewing 1996), with which coffinite is isostructural.

Essentially all reported analyses of natural coffinite indicate H_2O, and the structural role of H_2O has been long been debated (Mumpton and Roy 1961, Speer 1982b, Janeczek 1991). Infrared spectra of hydrothermally synthesized coffinite do not show evidence for OH groups, and no difference in X-ray powder diffraction patterns is observed between anhydrous and hydrous samples (Fuchs and Gebert 1958). H_2O groups in coffinite are believed to occupy open channels along [001] (Fig. 2), and are not believed to be an essential structural constituent (Janeczek 1991).

However, attempts to synthesize coffinite by using anhydrous high-temperature (~1000°C) methods have not been successful (e.g., Lunga 1966, Hanchar 1996).

In addition to U and Th, the tetravalent light actinides, Pa, Np, Pu, and Am also form zircon-type orthosilicates, and like $ThSiO_4$, $PaSiO_4$ is also dimorphous, with a monoclinic huttonite-type polymorph stable at elevated temperature (Speer 1982b). The degree of solid solution among isostructural actinide orthosilicates has not been studied in detail. Complete solid solution cannot be assumed based solely on similarities in ionic radii and valence (e.g., Begg et al. 2000, Burakov et al. 2002).

We should note that thorogummite, $(Th,U)SiO_4 \cdot nH_2O$, is an actinide orthosilicate mineral considered isostructural with zircon. Thorogummite is rather poorly described structurally and chemically (Speer 1982b, Gaines et al. 1997). It probably represents an intermediate in the solid solution between coffinite and thorite, and thorogummite may be superfluous as a mineral name (Finch and Murakami 1999).

Phosphates

Three naturally occurring REE phosphates, xenotime (YPO_4), xenotime-(Yb) ($YbPO_4$) and pretulite ($ScPO_4$), crystallize with the zircon structure (Boatner 2002), as well as several synthetic heavy-lanthanide orthophosphates (Ni et al. 1995) (Table 1). The structures of xenotime and the other zircon-group orthophosphates are topologically identical to zircon, with REE^{3+} ions occupying Zr-equivalent dodecahedral sites and P^{5+} occupying Si-equivalent tetrahedral sites (Ni et al. 1995). The polyhedral volume of the PO_4 tetrahedron in xenotime-type $REEPO_4$ orthophosphates is significantly smaller than the analogous SiO_4 tetrahedron in zircon, reflecting the smaller ionic radius of $^{[IV]}P^{5+}$ (0.15 Å) compared with $^{[IV]}Si^{4+}$ (0.26 Å). The polyhedral volume of the $REEO_8$ dodecahedron is correspondingly larger than the analogous ZrO_8 dodecahedron in zircon. Boatner (2002) reviews the structures, chemistry and physical properties of zircon-group REE phosphates in more detail.

Due to the lanthanide contraction (ionic radii of light lanthanides are larger than those of heavy lanthanides) orthophosphates of light lanthanides, La through Gd, crystallize with the monoclinic monazite structure (Ni et al. 1995), which is described in the section on related structures. Synthetic $BiPO_4$ possesses the monazite structure at low temperature (Schwarz 1963), as does the trivalent actinide phosphate $PuPO_4$ (Bjorklund 1958).

Borates

Two naturally occurring borates are known that possess the zircon structure, both of which share the general formula $(Ta,Nb)BO_4$. Behierite (Nb-rich) and schiavinatoite (Ta-rich) are both exceedingly rare, occurring in B-rich pegmatites (Mrose and Rose 1961, Demartin et al. 2001). Little is known about the stability of these minerals, although Bayer (1972) reported that synthetic $TaBO_4$ decomposes above 900°C to Ta_2O_5 with volatilization of B_2O_3. We are unaware of any studies on the extent of solid solution between zircon and the borates; however, minor Ta and Nb have been reported in zircon analyses, and B^{3+} is certainly a potential charge-compensating substituent (and one that is notably difficult to detect).

Vanadates

Three vanadate minerals possess the zircon structure: wakefieldite-(Y), YVO_4, wakefieldite-(Ce), $(Ce,Pb)VO_4$, and dreyerite, $BiVO_4$. The first description of wakefieldite-(Ce) (originally named kusuite) reported that it contained approximately equal proportions of di- and tetravalent Pb, as well as trivalent Ce (Deliens and Piret 1977), although Pb-free wakefieldite-(Ce) was subsequently described by Baudracco-Gritti et al. (1987). Synthetic $ScVO_4$ is isostructural with zircon (Schwarz 1963), and a complete series of lanthanide-bearing vanadates has been synthesized (Ce through Lu), all of which have the zircon structure (Durif 1956, Carron et al. 1958, Lohmüller

et al. 1973). $LaVO_4$ is the only REE orthovanadate with the monazite structure at room temperature and pressure (Stubican and Roy 1963, Schwarz 1963, Rice and Robinson 1976); however it adopts the zircon structure when synthesized hydrothermally (Oka et al. 2000).

Wakefield-(Y) contains 4-6 wt % each of heavy lanthanides (Dy, Yb, Er) and no measurable light lanthanides (Miles et al. 1971). Naturally occurring Pb-free wakefieldite-(Ce) contains several weight percent light lanthanides (up to Sm) and no measurable heavy lanthanides, although it does contain approximately 3 wt % Y (Baudracco-Gritti et al. 1987). Pb-bearing wakefieldite-(Ce) from Zaire reportedly contains no measurable REE other than Ce (Deliens and Piret 1977). Minor substitution by As and P for V is common in naturally occurring zircon-type vanadates, although to our knowledge complete solid solution has not been demonstrated between zircon-group vanadates and the isostructural arsenates or phosphates. Synthetic zircon-type REE vanadates transform to the scheelite structure between about 3.5 and 10 GPa, depending on temperature (Stubican and Roy 1963, Jayaraman et al. 1987, Mazhenov et al. 1988, Duclos et al. 1989, Range and Meister 1990).

Lattice parameters of zircon-type REE orthovanadates depend directly on the radius of the lanthanide ion (Chakoumakos et al. 1994) and can be described with the following polynomials: $a = 2.6809 + 6.3244\ R - 1.9221\ R^2$; $c = 6.2173 - 1.3048\ R + 1.3548\ R^2$, in which R is the effective ionic radius, in Ångströms, from Shannon (1976). The O atomic positional parameters depend linearly on the lanthanide-ion radius (Chakoumakos et al. 1994): $y = 0.4864 - 0.05126R$; $z = 0.1577 + 0.04269R$ (space group $I4_1/amd$, origin at $8c.2/m$). Several zircon-type REE orthovanadates (REE = Pr, Nd, Tb, Ho, Tm, Tb) exhibit anomalous thermal expansion caused by magnetoelastic effects (Kazei et al. 1995, Skanthakumar et al. 1995, Nipko et al. 1997, Bowen 1998). Elastic constants for zircon-type orthovanadates are not so well known; however, elastic constants have been reported for $TbVO_4$ (Melcher 1976), $DyVO_4$ (Sandercock et al. 1972, Melcher 1976), $HoVO_4$ and $ErVO_4$ (Hirano et al. 2002b). Bowden (1998) provides a detailed review of thermal properties of REE vanadates.

Dreyerite ($BiVO_4$) is trimorphous with the minerals pucherite and clinobisvanite. Dreyerite, which is isostructural with zircon, is found in rhyolitic ash-flow tuff (Dreyer and Tillmanns 1981), suggesting a high-temperature and (relatively) low-pressure genesis. Clinobisvanite is monoclinic ($I2/a$); it is not isostructural with monazite but possesses a "distorted scheelite structure" (Mariathasan et al. 1986). Pucherite is orthorhombic and also structurally related to scheelite (Qurashi and Barnes 1953). Clinobisvanite, the $BiVO_4$ polymorph stable at ambient temperature and pressure, transforms to the scheelite structure at elevated temperature or at pressures above 1.4 GPa (Hazen and Mariathasan 1982, Mariathasan et al. 1986). Synthetic clinobisvanite is ferroelastic, whereas the scheelite-type polymorph of $BiVO_4$ is paraelastic. The monoclinic-to-tetragonal transformation in $BiVO_4$ is purely displacive and readily reversible, involving small shifts of Bi and O atoms (Hazen and Mariathasan 1982), which probably explains why the low-pressure polymorph of $BiVO_4$ (clinobisvanite) is known as a mineral, whereas the high-pressure scheelite-type polymorph is not. As for clinobisvanite, the orthorhombic distortion that distinguishes pucherite from the scheelite-type polymorph involves relatively small atomic displacements (Qurashi and Barnes 1952, Mereiter and Preisinger 1986); however, the stability of pucherite relative to other $BiVO_4$ polymorphs is not known.

Arsenates

Chernovite ($YAsO_4$) is the only naturally occurring arsenate member of the zircon group (Goldin et al. 1967), although several synthetic zircon-type REE arsenates are also known. $REEAsO_4$ compounds containing heavy lanthanides (Sm through Lu), Y and Sc, crystallize with the zircon structure (Durif and Forrat 1957, Schwarz 1963), whereas the four light lanthanides La, Ce, Pr and Nd form orthoarsenates that are isostructural with monazite (Carron et al. 1958). This is consistent with the trend observed for the REE orthophosphates, except that the "break" between the

xenotime-type (zircon-type) and monazite-type structures occurs between Nd and Sm for REE arsenates, whereas it occurs between Gd and Tb for REE phosphates.

Synthetic $NdAsO_4$ possesses the monazite structure at room temperature and pressure but adopts the scheelite structure at elevated temperature and pressure (Mazhenov et al. 1988, Stubican and Roy 1963). Two naturally occurring orthoarsenates possess the monazite structure: gasparite-(Ce), $CeAsO_4$ (Graeser and Schwander 1987), and rooseveltite, $BiAsO_4$ (Herzenberg 1946, Schwarz 1963). The latter is dimorphous with tetrarooseveltite, which is isostructural with scheelite (Mooney 1948, Sejkora and Rídkošil 1994). Mooney (1948) noted that monoclinic $BiAsO_4$ (monazite structure) precipitates quickly when synthesized hydrothermally, whereas "long digestion periods tend to produce the tetragonal [scheelite-type] form."

Naturally occurring REE arsenates commonly exhibit As-V and As-P solid solution (Cabella et al. 1999), and a complete solid-solution series has been demonstrated between chernovite and xenotime (Graeser et al. 1973). Limited replacement of As by W is also reported. Paranite, $Ca_2Y(AsO_4)(WO_4)_2$, is an ordered derivative of the scheelite structure, with alternating layers of composition $CaWO_4$ and $YAsO_4$ in the ratio 2:1 (Demartin et al. 1992).

Chromates

Chromatite ($CaCrO_4$) is a rare chromate isostructural with zircon (Weber and Range 1996). The CaO_8 dodecahedron in chromatite is larger than the ZrO_8 dodecahedron in zircon, and the CrO_4 tetrahedron, which is also slightly larger than the SiO_4 tetrahedron in zircon, is less distorted than in zircon. This can be rationalized by there being less repulsion between Ca^{2+} and Cr^{6+} compared to Zr^{4+} and Si^{4+} in zircon.

To our knowledge, no other zircon-type compounds with Cr^{6+} are known, natural or synthetic. However, a full suite of zircon-type REE compounds with the general formula $REECrO_4$ (La through Lu) have been synthesized (Buisson et al. 1964). The three pentavalent cations, As^{5+}, Cr^{5+} and V^{5+} possess closely similar ionic radii in tetrahedral coordination (0.335-0.355 Å), so that $REECrO_4$, $REEVO_4$ and $REEAsO_4$ might be expected to form solid-solution series.

Related structures

Reidite is the naturally occurring high-pressure polymorph of $ZrSiO_4$. First synthesized in the laboratory (Reid and Ringwood 1969), reidite was discovered recently in zircon-bearing marine sediments in an impact-ejecta layer off the coast of New Jersey (Glass et al. 2002a,b). Reidite is tetragonal, space group $I4_1/m$, and is isostructural with scheelite ($CaWO_4$). Scheelite (and by inference reidite) shares several structural features with zircon. As for zircon, Si atoms in reidite occupy distorted SiO_4 tetrahedra and Zr atoms occur within ZrO_8 dodecahedra. ZrO_8 polyhedra in reidite share edges with adjacent ZrO_8 polyhedra, forming zigzag chains along <100>. These chains are crossed linked through SiO_4 tetrahedra by sharing corners with them (Fig. 8). Like zircon, there are two Zr-O distances in reidite, and the ZrO_8 dodecahedron can be described as two interpenetrating ZrO_4 tetrahedra: one elongated, ZrO_4^e, the other compressed, ZrO_4^c. Thus the reidite structure is composed of two interpenetrating "C-9 type" arrays of corner-sharing tetrahedra, as is zircon. Unlike zircon, however, *Zr* and *Si* polyhedra in reidite do not share edges, and the two C9-type arrays of tetrahedra are composed, not of SiO_4 and ZrO_4^c tetrahedra, but of SiO_4 and ZrO_4^e tetrahedra (Fig. 9). Also in contrast with zircon, the ZrO_4^c tetrahedra (which also share corners with SiO_4 tetrahedra) form layers of corner-sharing tetrahedra parallel to (001) in reidite, and these layers do not share polyhedral constituents with adjacent ZrO_4^c layers (Nyman et al. 1984). These differences in connectivity of the structures of reidite (scheelite) and zircon may explain observed differences in thermal expansion (Bayer 1972) and compressibility (Hazen and Finger 1979, Scott et al. 2002) for the two structure types.

Monazite ($CePO_4$) is the monoclinic form of $REEPO_4$ compounds adopted by light lanthanide orthophosphates (Ni et al. 1995, Boatner 2002). Although $ZrSiO_4$ does not form a poly-

morph with the monazite structure, thorite transforms at high pressure and temperature to huttonite (Dachille and Roy 1964), which is isostructural with monazite (Taylor and Ewing 1978). We discuss the monoclinic monazite/huttonite structure here in order to aid in our discussion of phase transformations in the next section.

Monazite is monoclinic, crystallizing in space group $P2_1/n$. The structure of monazite is similar to that of zircon in several important ways. In monazite, isolated PO_4 tetrahedra share corners and edges with CeO_9 polyhedra, which superficially resemble ZrO_8 dodecahedra in zircon. The *Ce* polyhedra in monazite share edges with each other to form chains parallel to the *a* axis (Fig. 10) that resemble analogous ZrO_8 dodecahedral chains in zircon (cf. Fig. 1). The Ce atom in monazite is coordinated by nine O atoms, described by Taylor and Ewing (1978) as four axial O atoms (two each forming the shared edge with two adjacent PO_4 tetrahedra) and five equatorial O atoms. The equatorial O atoms are each part of five neighboring PO_4 tetrahedra that share their corners with the *Ce* polyhedron. Thus, the Ce polyhedron in monazite shares corners and edges with seven neighboring PO_4 tetrahedra, whereas the ZrO_8 polyhedron in zircon shares polyhedral elements with six SiO_4 tetrahedra. The four axial O atoms define a distorted CeO_4 tetrahedron elongated along [001], analogous to the ZrO_4^e tetrahedron in zircon. The edge-sharing *P* and *Ce* polyhedral chains along [001] in monazite (Fig. 11) closely resemble the [001] polyhedral chains in zircon, although the chains in monazite are twisted compared to those in zircon (cf. Fig. 4).

As noted, the zircon structure can be visualized as two interpenetrating arrays of alternating, corner-sharing SiO_4 and ZrO_4^c tetrahedra (Fig. 5). Owing to nine O atoms being coordinated to Ce in monazite, the CeO_9 polyhedron cannot be adequately described as two interpenetrating tetrahedra. The ninth Ce-O bond in monazite can be seen as arising from a twisting of polyhedra in monazite relative to analogous polyhedra in zircon (compare Figs. 1, 10 and 4, 11), which results in an additional bond between a seventh PO_4 group and the CeO_9 polyhedron. The two C9-type arrays of SiO_4 and ZrO_4^c tetrahedra, which are independent in the zircon structure, are no longer

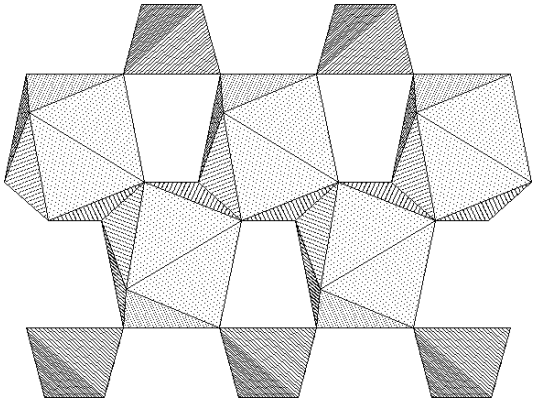

Figure 8. Scheelite structure projected on (100) with *c* axis vertical and *b* axis (a_2) horizontal. CaO_8 dodecahedra (ZrO_8 in reidite) are shaded light gray; WO_4 tetrahedra (SiO_4 in reidite) are striped.

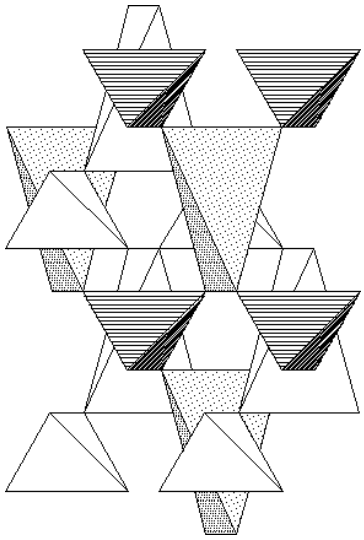

Figure 9. C9-type array of tetrahedra in the structure of scheelite: WO_4 (dark gray striped) and CaO_4^e (light gray stippled). (CaO_4^e and WO_4 tetrahedra in scheelite are equivalent to ZrO_4^e and SiO_4 tetrahedra, respectively, in reidite). Projection is approximately on (110) with *c* axis vertical and *b* axis (a_2) horizontal.

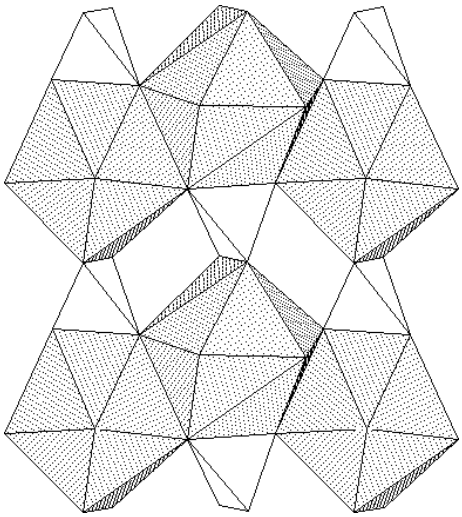

Figure 10. Monazite structure projected on (100); *c* axis is vertical, *b* axis is horizontal.

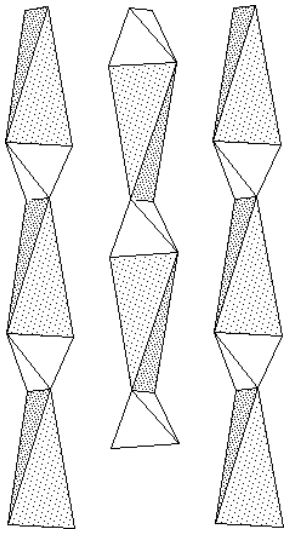

Figure 11. Monazite structure projected on (100), illustrating [001] chains of edge-sharing tetrahedra: CeO_4^e (light gray stippled) and PO_4 (no shading); *c* axis is vertical, *b* axis is horizontal (cf. Fig. 4).

independent in monazite, due to the ninth Ce-O bond. Thus, monazite has greater overall structural connectivity than does zircon. The structure of monazite is more densely packed and space-filling than zircon, and it lacks the interstitial voids and channels present in the zircon structure.

Rutile. Vegard (1916) originally reported that zircon was isostructural with rutile (tetragonal TiO_2), although he corrected this later (Vegard 1926). Despite the contention by Bragg and Claringbull (1965) that "there is no relation between the two structures," they can, in fact, be compared in a straightforward manner (Nyman et al. 1984). In zircon, Si and Zr atoms are coordinated by four and eight O atoms, respectively, whereas in rutile, Ti atoms are coordinated by six O atoms. Nyman et al. (1984) point out that each pair of Ti octahedra in rutile can be correlated to a pair of Zr and Si polyhedra in zircon through small displacements of four O atoms. The displacement relates two edge-sharing *Ti* octahedra to an edge-sharing pair of *Zr* and *Si* polyhedra. Thus, the [001] chains of edge-sharing *Zr* and *Si* polyhedra in zircon are analogous to the [001] chains of edge-sharing *Ti* octahedra in rutile.

Garnet. Robinson et al. (1971) compared the structures of zircon and garnet ($X_3Y_2T_3O_{12}$). Both structures contain chains of edge-sharing TO_4 tetrahedra and XO_8 dodecahedra. These chains are oriented along the three crystallographically equivalent [111] directions in garnet, forming cross-linked chains with octahedral interstices. These YO_6 octahedra are typically occupied by high field-strength cations, such as Al^{3+}, Fe^{3+} and Cr^{3+}, whereas the XO_8 dodecahedra are occupied by comparatively low field-strength cations such as Mg^{2+}, Ca^{2+}, Mn^{2+}, and Fe^{2+}.

Anhydrite. The structure of anhydrite ($CaSO_4$) is similar to that of zircon in several ways. The Ca^{2+} cation in anhydrite occupies a dodecahedron that is closely similar to the ZrO_8 dodecahedron in zircon (and the CaO_8 dodecahedron chromatite). These CaO_8 dodecahedra share edges with SO_4 tetrahedra, forming chains along [001] that strongly resemble the [001] chains in zircon. In addition, the CaO_8 dodecahedra share edges with adjacent CaO_8 dodecahedra along [100], also as seen in zircon. However, unlike the zircon structure, CaO_8 dodecahedra in anhydrite share only corners with neighboring CaO_8 dodecahedra along [010], thereby breaking the tetragonal symmetry. Anhydrite is orthorhombic, space group *Amma*, with a = 6.993 Å, b = 6.995 Å, c = 6.245 Å

(Hawthorne and Ferguson 1975), and the distortion from tetragonal is seen to be small. Nyman et al. (1984) describe this structural relationship in more detail.

STRUCTURAL EFFECTS OF TEMPERATURE, PRESSURE AND COMPOSITION

Temperature

The thermal expansion of zircon is quite low, with an average (bulk) coefficient of thermal expansion (β) of approximately 4.5×10^{-6}/°C. As would be expected from the structure, the thermal expansion of zircon is anisotropic, with expansion along [001] greater than along <100> ($\beta_{<100>} = 3.2 \times 10^{-6}$/°C and $\beta_{[001]} = 5.4 \times 10^{-6}$/°C, Bayer 1972). Bayer (1972) examined the thermal behaviors of several synthetic ATO_4 compounds with zircon and scheelite structures and found that the thermal expansion of compounds with the zircon structure is generally less than that of scheelite-type compounds, and that thermal expansion tends to increase with decreasing valence of dodecahedral-site cations.

Zircon is stable up to 1690°C (1963 K) at ambient pressure, at which point it decomposes to the constituent oxides. A neutron-diffraction study of zircon up to 1900 K (1627°C) found that zircon undergoes a displacive structural "transition" at approximately 1100 K (827°C), where there is a discontinuity in the thermal expansion of the *a* and *c* lattice parameters (Mursic et al. 1992). The temperature-dependence of lattice parameters *a* and *c* can be described, both above and below the 1100 K transition, by a second-degree polynomial: $A_0 = A_1T + A_2T^2$. Between room temperature and 1100 K, the polynomial coefficients are $A_0 = 6.6003$, $A_1 = 126 \times 10^{-7}$, $A_2 = 82 \times 10^{-10}$ for the *a* axis, and $A_0 = 5.9783$, $A_1 = 29 \times 10^{-6}$, $A_2 = 67 \times 10^{-10}$ for the ***c*** axis; whereas, between approximately 1500 and 1800 K, the polynomial coefficients for the temperature dependence of the *a* axis are $A_0 = 6.65$, $A_1 = -4 \times 10^{-5}$, $A_2 = 24 \times 10^{-9}$, and those for the *c* axis are $A_0 = 6.05$, $A_1 = -5 \times 10^{-5}$, $A_2 = 24 \times 10^{-9}$ (Mursic et al. 1992).

Volume expansion during heating of zircon is due primarily to expansion of the ZrO_8 dodecahedron, there being relatively little change in the SiO_4 tetrahedral volume below 1100 K. Increased dodecahedral volume correlates with an increase in the longer Zr-O distance, corresponding to the elongated ZrO_4^e tetrahedron, which shares edges with SiO_4 tetrahedra. Relatively little change in the shorter Zr-O bonds or the volume of the compressed ZrO_4^c tetrahedron occurs up to the 1100 K transition. Between 1100 and 1200 K, the SiO_4 tetrahedron undergoes a sharp increase in volume due to an increase in the Si-O bond length from 1.622 Å to 1.628 Å (Mursic et al. 1992). The corner-sharing tetrahedra (SiO_4 and ZrO_4^c) respond to these changes in SiO_4 volume through rotation, leaving the longer Zr-O distance essentially unchanged through the transition. The edge-sharing ZrO_4^e tetrahedron cannot rotate (independent of the SiO_4 tetrahedron), and the longer Zr-O bonds must, therefore, lengthen continuously during and following expansion of the Si-O bond. By approximately 1500°C, the geometry of the SiO_4 tetrahedron approaches that of an ideal tetrahedron (O-Si-O angle = 109°). Mursic et al. (1992) explain the decomposition of zircon by the gradual breakdown of the ZrO_8 dodecahedral polyhedron due to increasing incompatibility of the two interpenetrating ZrO_4 tetrahedra. Thus, the thermal decomposition of $ZrSiO_4$ to (tetragonal) ZrO_2 and SiO_2 (beta-cristobalite) can be described as a structural rearrangement of the ZrO_8 polyhedron, which is no longer compatible with the SiO_4 polyhedron. The SiO_4 tetrahedra eventually rearrange, crystallizing beta-cristobalite (Mursic et al. 1992, Colombo et al. 1999).

The thermal behavior of zircon contrasts with that of thorite, which transforms to the high-temperature polymorph huttonite before decomposing to ThO_2 and SiO_2 (Dachille and Roy 1964, Finch et al. 1964). Huttonite, which has the monazite structure, shares some important structural features with thorite (zircon structure); however, Th in huttonite is coordinated by nine O atoms, rather than eight as in thorite, and the ThO_9 polyhedron in huttonite shares corners with seven SiO_4 tetrahedra, rather than six as in thorite (Taylor and Ewing 1978). The structural change is

accomplished through rotations of ThO_4^e and SiO_4 tetrahedra and formation of an additional bond between an O atom of the fifth SiO_4 tetrahedron and the *Th* site. The transformation of thorite to huttonite results in a structure with greater overall connectivity than zircon, which, as noted, consists of two independent arrays of *Si* and *Zr* tetrahedra. These arrays both exist in huttonite, but they are not independent, being connected through the additional Th-O-Si linkage. The structure collapses slightly due to the rotation of polyhedra and the additional Th-O bond. The transformation of thorite to huttonite is sluggish, presumably due to formation of an additional Th-O bond. Details of the transformation remain unclear, as no high-temperature structural studies of the thorite-huttonite transformation have, to our knowledge, been reported. The fact that a structural transformation similar to the thorite-huttonite transformation is not observed in zircon before decomposition may be due to the greater tetrahedral rotation required to increase the coordination number around the small Zr^{4+} cation.

Coffinite ($USiO_4$) is isostructural with thorite and zircon (Fuchs and Gebert 1958). The phase stability of coffinite remains largely uncertain. High-temperature synthesis experiments (e.g., Lunga 1966) suggest that coffinite is metastable relative to $UO_2 + SiO_2$. However, coffinite occurs primarily in low-temperature sedimentary rocks (Plant et al. 1999) and formation of coffinite at low temperatures may be kinetically inhibited on laboratory timescales. Considering the similar ionic radii of $^{[VIII]}U^{4+}$ (1.00 Å) and $^{[VIII]}Th^{4+}$ (1.05 Å), a high-temperature polymorph of $USiO_4$ analogous to huttonite might be expected; however, such a phase has never been reported in laboratory experiments or from natural samples. The reason for this apparent disparity between coffinite and thorite is not clear.

Pressure

Hazen and Finger (1979) determined the bulk modulus (K_{0T}) for natural zircon from crystal-structure refinements up to 4.8 GPa, reporting values of 227 GPa or 234 GPa, depending on the assumed value for the isothermal pressure derivative, K_{0T}' ($K_{0T}' = 6.5$ and 4, for the low and high values, respectively). This makes zircon one of the most incompressible silicate minerals known, with a bulk modulus similar to those of perovskite-type structures and silicates with Si in octahedral coordination (Knittle 1995). Crocombette and Ghaleb (1999) calculated the bulk modulus for pure $ZrSiO_4$, deriving a value of 245 GPa, in excellent agreement with the value reported by Hazen and Finger (1979). Recently, van Westrenen et al. (2003a) measured unit-cell volumes of pure, synthetic zircon up to 27 GPa and report a bulk modulus of 201 GPa (K′ of 4.0), significantly lower than the value reported by Hazen and Finger (1979) for natural zircon.

The bulk modulus of the SiO_4 tetrahedron (230 ± 40 GPa) is low compared to other silicates, whereas that of the ZrO_8 dodecahedron (280 ± 40 GPa) is anomalously high for a polyhedron with coordination number greater than six (Hazen and Finger 1979). Smyth et al. (2000) suggest that the *Zr* polyhedron largely accounts for the remarkable incompressibility of zircon, attributing this to the high valence and relatively large ionic radius of Zr^{4+} (0.84 Å). As for its thermal expansion, zircon exhibits anisotropic compressibility, being about 70% more compressible along [001] than along <100> (Hazen and Finger 1979). This is explained by the fact that the four short Zr-O bonds (corresponding to the ZrO_4^c tetrahedron), which are sub-parallel to the (001) plane, are less compressible than the longer Zr-O bonds, which are closer to being parallel to [001] (Smyth et al. 2000).

Zircon transforms at high pressure to reidite, which is isostructural with scheelite. The transformation is believed to occur via a martensitic-type transformation (Kusaba et al. 1985, 1986; Leroux et al. 1999). Crystallographically, the structure of reidite can be derived by simultaneously twinning the zircon structure on (200), (020) and (002) (Nyman et al. 1984). Deformation in experimentally shock-metamorphosed zircon crystals is dominated by planar deformation features, interpreted as micro-twins predominantly on (100), (010) and (111), as well as amorphous planar deformation features (Leroux et al. 1999). Experimentally, Kusaba et al. (1986) concluded

that the [110] direction in zircon becomes the [100] direction in reidite during the shock-induced transformation zircon to reidite, a conclusion consistent with a transmission electron microscope study of experimentally shocked zircon crystals, in which the [110] direction of reidite is observed to be parallel to the [100] direction in adjacent zircon (Leroux et al. 1999). The latter study also revealed that the (112) plane in reidite parallels the (100) plane of zircon in shocked crystals. These observations suggest an epitaxial relationship between zircon and reidite.

The transformation of zircon to reidite is sluggish and the equilibrium transition pressure is not well constrained. The transition pressure at 1300 K (1027°C) is reportedly 12 GPa (Liu 1979), and if the Clapyron slope of the zircon-reidite phase boundary is positive, the room-temperature transition pressure must be lower than this. Crocombette and Ghaleb (1998) calculated an equilibrium transition pressure of 5 GPa (at 0 K) by using both empirical potentials and *ab initio* electronic-structure calculations. High-pressure shock and static experiments reveal a rather wide range of observed room-temperature transformation pressures consistently above about 20 GPa (Kusaba et al. 1985, Knittle and Williams 1993, Fiske et al. 1994, Leroux et al. 2001). A recent high-pressure diamond-anvil X-ray powder-diffraction study on the room-temperature compressibility of pure synthetic zircon reports evidence for reidite in powder-diffraction patterns from zircon crystals exposed to just under 20 GPa (van Westrenen et al. 2003a), about 3 GPa lower than the previously reported transition pressure observed for natural zircon (Knittle and Williams 1993). van Westrenen et al. (2003a) suggest that low concentrations of impurities in natural zircon crystals might affect compressibilities and observed transition pressures, a contention that appears to be supported by a recent study of room-temperature compressibility of synthetic zircon crystals doped with approximately 10 wt % REE + P (van Westrenen et al. 2003b). That study reports that the compressibility of REE+P-doped zircon is significantly greater than for pure $ZrSiO_4$, and that evidence for the onset of the zircon-reidite transition is not observed below 22.5 GPa.

As for its temperature dependence, the pressure-dependent behavior of thorite contrasts with that of zircon. The high-pressure polymorph of $ThSiO_4$ is huttonite (which is also the high-temperature $ThSiO_4$ polymorph). The transformation from thorite to huttonite reflects a rotation of tetrahedra such that the coordination number of Th increases from eight in thorite to nine in huttonite, which, as discussed in the section on temperature effects, leads to an increase in structural connectivity in huttonite compared to thorite and a more compact structure.

Huttonite is more dense and has lower symmetry than thorite, which is unusual for a high-temperature polymorph. The Clausius-Clapyron equation relates differences in volumes and entropy across a phase boundary to the slope of the phase boundary in P-T space:

$$dP/dT = (S_i\text{-}S_j)/(V_i\text{-}V_j) = \Delta S/\Delta V \quad (1)$$

Based on their relative densities, molar volumes of the three structure types decrease in the order $V_{Zirc} > V_{Mon} > V_{Sch}$, since, for a given composition, density for each structure type increases in the order $D_{Zirc} < D_{Mon} < D_{Sch}$. Based on the symmetries of these three structure types, molar entropies might be expected to decrease in the order $S_{Zirc} > S_{Sch} > S_{Mon}$, since higher symmetry tends to imply greater entropy. Using these arguments, we can postulate the Clapyron slope for phase boundaries between pairs of structure types zircon-scheelite, zircon-monazite and monazite-scheelite.

The phase boundary between zircon-type structures and scheelite-type structures is characterized by $V_{Sch} < V_{Zirc}$, and $S_{Sch} < S_{Zirc}$, making ΔV and ΔS both negative, so that $\Delta V/\ \Delta S$ and, therefore, dP/dT is positive; that is, the Clapyron slope is positive. Although the zircon-to-reidite transition is not well known, the slope of the analogous phase boundary between zircon-type and scheelite-type polymorphs of synthetic $HoVO_4$ is positive (Fig. 12), with the zircon-type polymorph stable at higher temperature and lower pressure than the scheelite-type polymorph (Stubican and Roy 1963), consistent with our expectation.

For the phase boundary between monazite-type and scheelite-type structures we can expect $S_{Sch} > S_{Mon}$ and $V_{Mon} > V_{Sch}$, making ΔS positive but ΔV negative, so that dP/dT will be negative for this phase boundary. This, too, is consistent with experiment. The P-T phase boundary between the monazite-type and the scheelite-polymorphs of $NdAsO_4$ has a negative slope (Fig. 13), with the scheelite-type polymorph stable at higher temperature and pressure (Stubican and Roy 1963).

The phase boundary between zircon-type and monazite-type structures has $V_{Zirc} > V_{Mon}$, and symmetry suggests that $S_{Zirc} > S_{Mon}$, making ΔV and ΔS both positive and, therefore, dP/dT positive. Of course, a well-known example of this phase boundary is that between thorite and huttonite, which has a *negative* Clapyron slope (Dachille and Roy 1964), contrary to our expectation (Fig. 14). The unit-cell volume of huttonite is less than that of thorite, so it seems clear that ΔV is negative. The negative Clapyron slope of the huttonite-thorite phase boundary, therefore, requires that the molar entropy of huttonite be greater than that of thorite ($\Delta S > 0$), which is counterintuitive given that huttonite is the lower-symmetry phase. Zircon-type $CeVO_4$ also transforms to the monazite-type structure at elevated temperature and pressure (Fukunaga and Yamaoka 1979); however, the pressure and temperature dependence of this transformation is not known.

It seems notable that the room-temperature polymorph of synthetic $ThGeO_4$ adopts the scheelite structure, transforming to the zircon-type structure above approximately 1100°C (Bayer 1972, Ennaciri et al. 1986). This is consistent with $HoVO_4$ but in apparent contrast with the observed behavior of $ThSiO_4$, which has no known scheelite-type polymorph. Studies of the thorite-huttonite transition have not been reported for pressures above 5 GPa (Dachille and Roy 1964), and whether huttonite might transform to a scheelite-type polymorph at higher pressures (as for $NdAsO_4$) is not known.

Experimental evidence from a variety of ATO_4 systems indicates that, for a given temperature, the polymorphic sequence with increasing pressure is *Zircon* → (*Monazite*) → *Scheelite*, where the (*Monazite*) signifies that zircon-type polymorphs of many ATO_4 compounds transform directly to the scheelite structure (this is, in fact, the more commonly observed transformation). The polymorphic sequence at fixed pressure and increasing temperature is more ambiguous. The

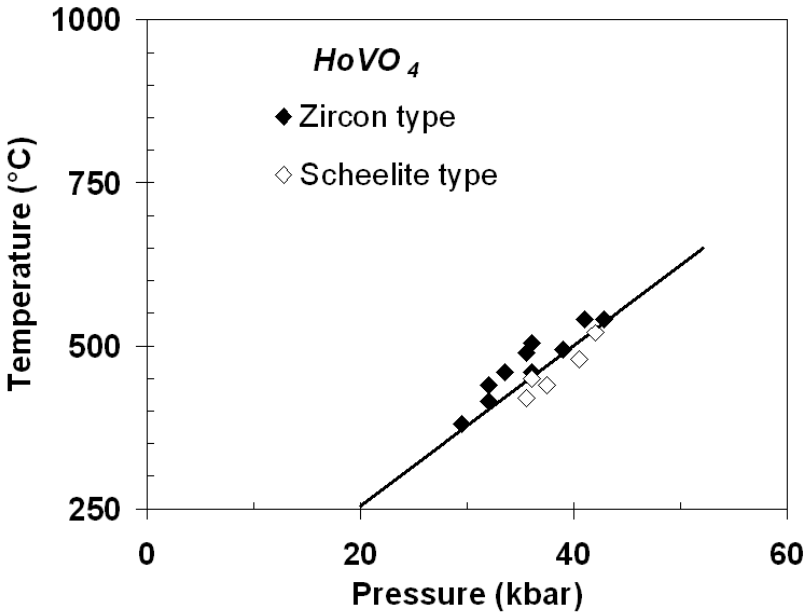

Figure 12. Plot of phase boundary between zircon-type and scheelite-type polymorphs of $HoVO_4$ reported by Stubican and Roy (1963). Positive Clapyron slope is consistent with expectation (see text).

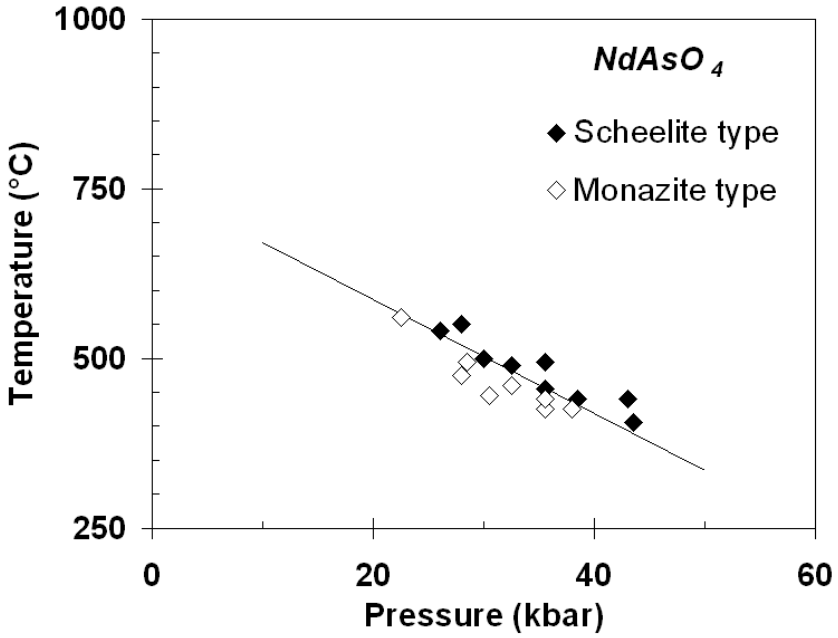

Figure 13. Plot of phase boundary between monazite-type and scheelite-type polymorphs of $NdAsO_4$ reported by Stubican and Roy (1963). Negative Clapyron slope is consistent with expectation (see text).

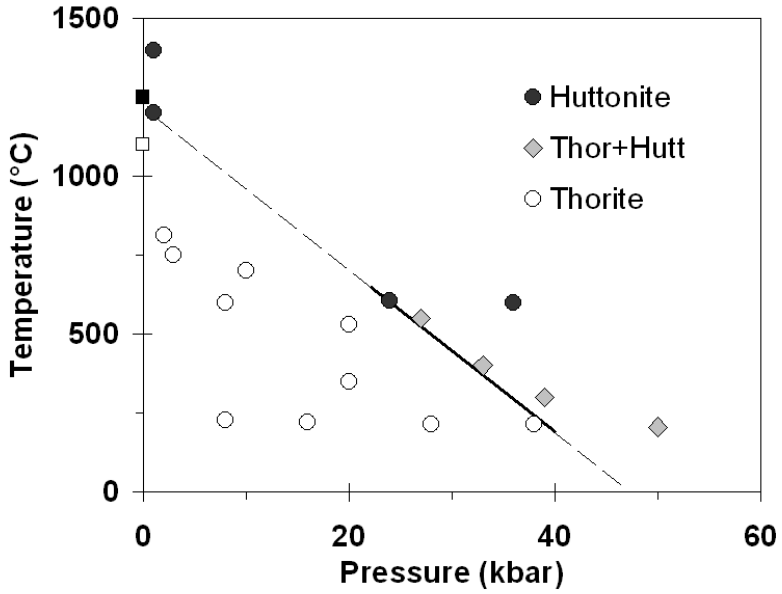

Figure 14. Plot of phase boundary between thorite and huttonite from data reported by Dachille and Roy (1964) (circles and diamonds). Squares correspond to synthesis temperatures at 1 bar reported by Taylor and Ewing (1978) for thorite (hollow square 1100°C) and huttonite (filled square 1250°C). Estimated phase boundary is drawn through 1215°C at 1 bar, which is within error of the equilibrium transition temperature reported by Finch et al. (1964): 1225(10)°C. Negative Clapyron slope is contrary to expectation based on changes in density and symmetry (see text).

most likely polymorphic sequence at constant pressure and increasing temperature seems to be *Monazite* → *Scheelite* → *Zircon*, based largely on the study of Stubican and Roy (1963); however, the isobaric transformation *Zircon* → *Monazite* is also known (for $ThSiO_4$, although the thorite-huttonite transformation may be anomalous). Thus, for a given ATO_4 composition, the scheelite-type structure is stable at the highest pressures and the zircon-type structure is apparently stable at the lowest pressures. The monazite-type structure is stable at either low temperature and intermediate pressure or at low pressure and intermediate temperature.

This ambiguity in the relative position of the stability field for monazite-type structures, as well as uncertainty about whether the thorite-huttonite phase boundary is representative of other zircon-type-to-monazite-type transformations, present a significant problem when evaluating potential pressure-temperature relationships among the three ATO_4 structure types. A schematic P-T phase diagram, based on experimental results from different ATO_4 systems, helps to illustrate the problem (Fig. 15). Figure 15 places the stability range of monazite-type structures at low temperatures and intermediate pressures, making zircon-type structures stable at all temperatures for pressures below the triple point. If the thorite-huttonite phase boundary is representative of analogous phase boundaries in other ATO_4 systems, phase boundaries between zircon-type structures and their higher-temperature polymorphs form an obtuse angle about the triple point, a violation of thermodynamic principles (the same problem arises if we assume that monazite-type structures are stable at high temperature and low pressure, upper left of diagram in Fig. 15, although this choice is considerably more difficult to rectify with expected Clapyron slopes discussed above). It appears that the thorite-huttonite phase boundary may well be anomalous among ATO_4 compounds. Of course, Clapyron slopes for phase boundaries indicated in Figure 15 can change significantly as a function of the ATO_4 system under consideration (possibly including whether they are positive or negative), and the degree to which solid solution and impurities might shift phase boundaries is unknown and potentially large. Additional high-pressure and high-temperature studies of ATO_4 compounds, especially $ThSiO_4$, $ThGeO_4$ and perhaps $Th(Si,Ge)O_4$ solid solutions, could help clarify P-T relationships among zircon-, scheelite- and monazite-type structures.

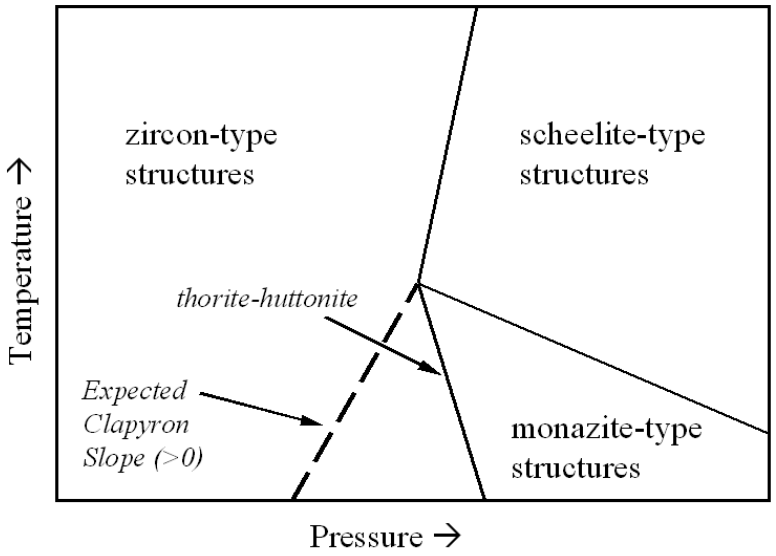

Figure 15. Hypothetical schematic phase diagram for ATO_4 compounds. Bold lines indicate phase boundaries between selected pairs of zircon-, scheelite-, and monazite-type ATO_4 compounds discussed in the text. The experimentally determined thorite-huttonite phase boundary is indicated. Also indicated is the expected positive Clapyron slope of that phase boundary (dashed line) based on changes in density and symmetry (see text).

Composition

Analyses of zircon commonly report trace amounts (or more) of P, Y, Hf, U, Th, and lanthanides (Hoskin and Schaltegger, this volume). Substitution of minor constituents into zircon has been studied by several workers (Caruba et al. 1995, Hanchar et al. 2001a), and the potential role of substitutions on the pressure dependence of the zircon structure was mentioned (van Westrenen et al. 2003b). Structural strain imposed by impurities replacing Zr and Si in zircon may affect how trace elements are incorporated into zircon (e.g., Brice 1975). Given the important role that zircon has assumed in geochemical and chronological studies, a clearer understanding of structural changes caused by substitutions may elucidate strain-imposed limits on trace-element substitutions (Hoskin 2000, Finch et al. 2001a, Hanchar et al. 2001b) and may lead to more predictive models for trace-element substitution in zircon and other minerals (Blundy and Wood 1994, Allan et al. 2001, Hanchar et al. 2001c, van Westrenen et al. 2001).

Zircon is commonly enriched in Y and heavy lanthanides relative to light and middle lanthanides (Hinton and Upton 1991, Belousova et al. 1998, Hanchar et al. 2001a, Hoskin and Schaltegger, this volume). REE-bearing zircon crystals commonly contain P, and owing to crystal-chemical similarities between Y^{3+} and heavy REE^{3+}, replacement of Zr^{4+} by REE^{3+} in zircon is commonly explained by the coupled xenotime-type substitution, in which P^{5+} replaces Si^{4+}, maintaining charge balance. Thus the ideal formula for xenotime-substituted zircon is $REE_xZr_{1-x}P_xSi_{1-x}O_4$, in which x indicates the mole fraction of the xenotime component. Implicit in the xenotime substitution is the assumption that P^{5+} replaces Si^{4+} at the tetrahedral site and REE replace Zr^{4+} at the dodecahedral site.

If xenotime substitution is the only mechanism by which charge balance is maintained in REE-substituted zircon, the atomic ratio REE:P must be unity. However, atomic ratios of REE:P measured in natural and synthetic zircon crystals commonly deviate significantly from one (Hinton and Upton 1991, Maas et al. 1992, Hoskin et al. 2000, Hanchar et al. 2001a), indicating a more complex charge-balance mechanism (or multiple mechanisms). Natural zircon crystals may exhibit charge-preserving substitutions besides, or in addition to, xenotime substitution, including exchange of OH^- groups for O^{2-} ions and coupled substitutions on the *Zr* site (Speer 1982a, Caruba et al. 1985, Hinton et al. 2003). Moreover, some degree of solid solution can be expected between zircon and the large number of isostructural zircon-group compounds discussed here.

A recent study of synthetic zircon crystals doped with REE and P revealed slight excesses of *Zr*-site cations (Zr and REE) that correlate with slight deficits in *Si*-site cations (Si and P) (Hanchar et al. 2001a) suggesting that minor Zr might substitute at the *Si* site (ionic radius of $^{[IV]}Zr$ is 0.59 Å), which is supported qualitatively by single-crystal X-ray diffraction data (Finch et al. 2001a). Examination of these same crystals by EXAFS confirmed that REE occupy the *Zr* site (Finch et al. 2001b). No evidence for interstitial REE was found from either X-ray diffraction data (Finch et al. 2001a) or X-ray absorption spectroscopy (Finch et al. 2001b).

Substitution of REE and P into zircon increases Zr-O bond distances and decreases Si-O bond distances (Finch et al. 2001a), consistent with the expected xenotime substitution. With increasing REE concentration, bond distances in substituted zircon crystals increase most sharply for the short Zr-O bond, whereas the long Zr-O bond distance (Zr-O') increases more gradually (Fig. 16); however, both Zr-O bond distances display maximum strain for Er-doped zircon, despite the fact that REE concentrations in Y and Yb crystals were greater than in Er-doped crystals. This is explained by the decreasing radii of REE, so that heavy lanthanides and Y (HREE) are increasingly compatible in the *Zr* site and, therefore, impart proportionately less strain in REE-substituted crystals than do light lanthanides (Finch et al. 2001a). Because P is incorporated along with REE (maintaining charge balance), the Si-O bond distance decreases monotonically as HREE concentration increases (Fig. 16). Finch et al. (2001a) concluded that strain at the *Si* site, caused by increased P substitution, explains the inability of zircon crystals to incorporate sufficient addi-

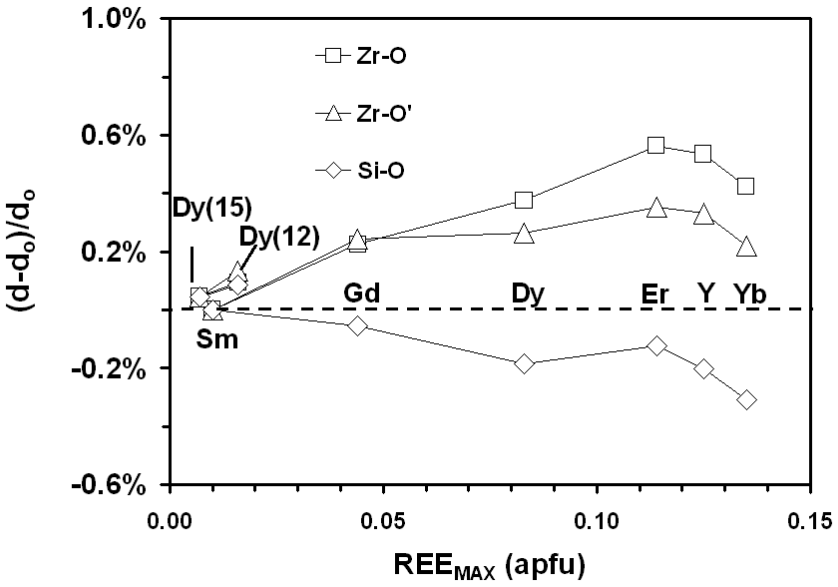

Figure 16. Change in cation-oxygen bond lengths (relative to equivalent bond distance in Sm-doped crystal) as a function of increasing REE in synthetic zircon crystals. Zr-O corresponds to the shorter Zr-O bond length; Zr-O' corresponds to the longer Zr-O bond length; "*apfu*" = atoms per formula unit; i.e., the value of x in $REE_xZr_{1-x}P_xSi_{1-x}O_4$ (after Finch et al. 2001a).

tional P^{5+} to charge balance continued incorporation of REE, despite the increased compatibility of HREE in the zircon structure. Strain induced by substitutions at both the *Zr* and *Si* sites in zircon helps explain why complete solid solution between zircon and xenotime has not been observed in synthetic crystals. By comparing analyses of natural zircons in xenotime-saturated rocks with preliminary results from an experimental study, Tomaschek and Ballhaus (2003) estimate that the apparent limit on xenotime substitution in zircon is approximately 10 mol % YPO_4.

As noted previously, the only refineable atomic positional parameters in zircon are the fractional coordinates of the *O* site: *y* and *z*. As REE and P increase in synthetic zircon crystals, the *O* site shifts parallel to {100}, approximately along <012>. The *O* site shifts away from the two neighboring *Zr* sites and towards (though not directly towards) the *Si* site, reflecting expansion of the REE-substituted ZrO_8 dodecahedron and concomitant contraction of the P-substituted SiO_4 tetrahedron. The observed shift in the O position in (REE+P)-doped zircon crystals trends in the direction of *O* positions reported for pure synthetic xenotime-type $REEPO_4$ compounds (Ni et al. 1995) (Fig. 17). It would be instructive to dope xenotime-type REE orthophosphates with Zr and Si (in addition to [REE+P]-doped zircon; e.g., Hanchar et al. 2001a, Tomaschek and Ballhaus 2003) in order to better constrain the extent of miscibility among these isostructural compounds. It seems likely that strain introduced by the substitution $(REE^{3+})_{+1}(P^{5+})_{+1}(Zr^{4+})_{-1}(Si^{4+})_{-1}$ is likely to be the most important factor limiting solid solution between zircon and xenotime.

ACKNOWLEDGMENTS

We are grateful for helpful reviews by Wim van Westrenen and Paul Hoskin, and for comments on phase transformations by Mats Hillert (KTH). Support to RJF was provided by Argonne National Laboratory under Contract No. W-31-109-ENG-38 with the U.S. Department of Energy, and through a grant from the Department of Energy Environmental Management Science Programs.

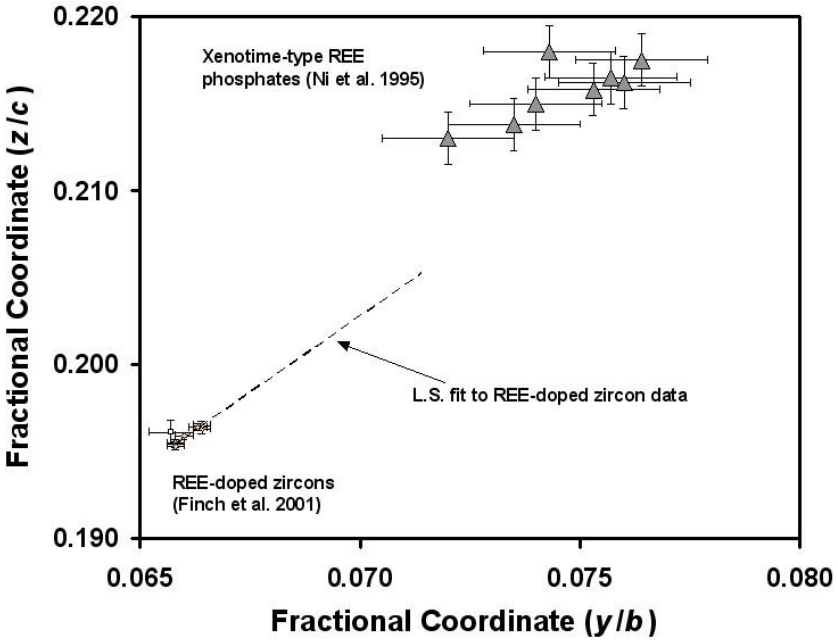

Figure 17. Plots of fractional coordinates *y* and *z* in synthetic zircon crystals doped with REE and P (Finch et al. 2001a) and in xenotime-type $REEPO_4$ crystals (Ni et al. 1995).

REFERENCES

Allan NL, Blundy JD, Purton JA, Lavrentiev My, Wood BJ (2001) Trace element incorporation in minerals and melts. *In* Solid Solutions in Silicate and Oxide Systems. Notes in Mineralogy, Geiger CA (ed) European Mineral Union, Eötvös University Press, 3:251-302

Baudracco-Gritti C, Quartieri S, Vezzalini G, Permingeat F, Pillard F, Rinaldi R (1987) A non plumboan wakefieldite-(Ce): New data on the mineral species corresponding to cerium orthovanadate. Bull Minéral 110:657-663

Bayer G (1972) Thermal expansion of ABO_4 compounds with zircon and scheelite structures. J Less Common Metals 26:255-262

Begg BD, Hess NJ, Weber WJ, Conradson SD, Schweiger MJ, Ewing RC (2000) XAS and XRD study of annealed ^{238}Pu- and ^{239}Pu-substituted zircons ($Zr_{0.92}Pu_{0.08}SiO_4$). J Nucl Mater 278:212-234

Belousova EA, Griffith WL, Pearson NJ (1998) Trace element composition and cathodoluminescence properties of Southern African kimberlitic zircon. Mineral Mag 62:355-366

Bernard F, Walter F, Ettinger K, Taucher J, Mereiter K (1998) Pretulite, $ScPO_4$, a new scandian mineral from the Styrean and Lower Austrian lazulite occurrences, Austria. Am Mineral 83:625-630

Bjorklund CW (1958) The preparation of PuP_2O_7 and $PuPO_4$. J Am Chem Soc 79:6347-6350

Blundy J, Wood B (1994) Prediction of crystal-melt partition coefficients from elastic moduli. Nature 372:452-454

Boatner LA (2002) Synthesis, structure, and properties of monazite, pretulite, and xenotime. Rev Mineral Geochem 48:87-121

Bowden GJ (1998) A review of the low temperature properties of the rare earth vanadates. Austral J Phys 51:201-236

Bowring SA (1995) The Earth's early evolution. Science 269:1535-1540

Bowring SA, Williams IS (1999) Priscoan (4.00-4.03 Ga) orthogneisses from northwestern Canada. Contrib Mineral Petrol 134:3-16

Bowring SA, Erwin DH, Jin YG, Martin MW, Davidek K, Wang W (1998) U/Pb zircon geochronology and tempo of the end-Permian mass extinction. Science 280:1039-1045

Bowring SA, Williams IS, Compston W (1989) 3.96 Ga gneisses from the Slave Province, Northwest Territories, Canada. Geology 17:971-975

Bragg L, Claringbull GF (1965) Crystal Structures of Minerals. Bell, London, p 113

Brice JC (1975) Some thermodynamic aspects of the growth of strained crystals. J Crystal Growth 28:249-253
Buick R, Thornett JR, McNaughton NJ, Smith JB, Barley ME, Savage M (1995) Record of emergent continental crust similar to 3.5 billion years ago in the Pilbara craton of Australia. Nature 375:574-575
Buisson G, Bertaut F, Mareschal J (1964) Étude cristallographique des composés $TCrO_4$ (T = terre rare ou Y). C R Acad Sci Paris 259:411-413
Burakov BE, Hanchar JM, Zamoryanskaya MV, Garbuzov VM, Zirlin VA (2002) Synthesis and investigation of Pu-doped single crystal zircon, $(Zr,Pu)SiO_4$. Radiochim Acta 89:1-3
Burakov BE, Hanchar JM, Zamoryanskaya MV, Anderson EB, Garbuzov VM, Kitsay AA, Krivovichev SV (2003) Investigation of single crystal zircon, $(Zr,Pu)SiO_4$, doped with ^{238}Pu. Radiochimica Acta (in press)
Cabella R, Lucchetti G, Marescotti P (1999) Occurrence of LREE- and Y-arsenates from a Fe-Mn deposit, Liguruan Briançonnais Domain, maritime Alps, Italy. Can Mineral 37:961-972
Carron MK, Mrose ME, Murata KJ (1958) Relation of ionic radius to structures of rare-earth phosphates, arsenates, and vanadates. Am Mineral 43:985-989
Caruba R, Baumer A, Ganteaume M, Iacconi P (1985) An experimental study of hydroxyl groups and water in synthetic and natural zircons: a model of the metamict state. Am Mineral 70:1224-1231
Caruba R, Baumer A, Ohnenstetter D, Cesbron F, Rouer O, Blanc P (1995) The hydrothermal synthesis of molybdenum, sulfur-doped zircon: a study of charge compensation mechanisms. Neues Jahrb Mineral Mh 1995:241-254
Chakoumakos BC, Abraham MM, Boatner LA (1994) Crystal structure refinements of zircon-type MVO_4 (*M* = Sc, Y, Ce, Pr, Nd, Tb, Ho, Er, Tm, Yb, Lu). J Sol State Chem 109:197-202
Colombo M, Chrosch J, Biagini R, Memmi I (1999) An IR analysis of the role of SiO_4 tetrahedra in thermally annealed $ZrSiO_4$. Neues Jahrb Mineral Monatsh 1999:113-122
Crocombette J-P (1999) Theoretical study of point defects in crystalline zircon. Phys Chem Minerals 27:138-143
Crocombette J-P, Ghaleb D (1998) Modeling the structure of zircon ($ZrSiO_4$): Empirical potentials, *ab initio* electronic structure. J Nucl Mater 257:282-286
Dachille F, Roy R (1964) Effectiveness of shearing stresses in accelerating solid-phase reactions at low temperature and high pressure. J Geol 72:243-247
Deliens M, Piret P (1977) La kusuite, $(Ce^{3+},Pb^{2+},Pb^{4+})VO_4$, nouveau mineral. Bull Soc Fr Minéral Cristallogr 100:39-41
Demartin F, Gramaccioli CM, Pilati T (1992). Structure of a new natural tungstate arsenate, $[Ca_2Y(AsO_4)(WO_4)_2]$, structurally related to scheelite. Acta Crystallogr C 48:1357-1359
Demartin F, Diella V, Gramaccioli CM, Pezzotta F (2001) Schiavinatoite, $(Nb,Ta)BO_4$, the Nb analogue of behierite. Eur J Mineral 13:159-165
Dreyer G, Tillmanns E (1981) Dreyerite, natural, tetragonal bismuth vanadate from Hirschhorn, Pfalz. Nueus Jahrb Mineral Monatsh 1981:151-154
Duclos SJ, Jayaraman A, Espinosa GP, Cooper AS, Maines RG (1989) Raman and optical absorption studies of the pressure-induced zircon to scheelite structure transformation in $TbVO_4$ and $DyVO_4$. J Phys Chem Solids 50:769-775
Durif A (1956) Structure et valence de $VCeO_4$. Acta Crystallogr 9:471
Durif A, Forrat F (1957) Sur quelques arsénates des terres rares à structure zircon. C R Acad Sci Paris 245:1636-1638
Ennaciri A, Kahn A, Michel D (1986) Crystal structures of $HfGeO_4$ and $ThGeO_4$ germanates. J Less-Common Metals 124:105-109
Ewing RC (1999) Nuclear waste forms for actinides. Proc Nat Acad Sci 967:3432-3439
Ewing RC, Lutze W (1997) Disposing of plutonium. Science 275:737
Fayek M, Janeczek J, Ewing RC (1997) Mineral chemistry and oxygen isotopic analyses of uraninite, pitchblende and uranium alteration minerals from the Cigar Lake deposit, Saskatchewan, Canada. Appl Geochem 12:549-565
Fayek M, Kyser K (1997) Characterization of multiple fluid-flow events and rare-earth-element mobility associated with formation of unconformity-type uranium deposits in the Athabasca basin, Saskatchewan. Can Mineral 35:627-658
Finch RJ, Murakami T (1999) Systematics and paragenesis of uranium minerals. Rev Mineral 38:91-179
Finch CB, Harris LA, Clark GW (1964) The thorite-huttonite phase transformation as determined by growth of synthetic thorite and huttonite single crystals. Am Mineral 49:782-785
Finch RJ, Hanchar JM, Hoskin PWO, Burns PC (2001a) Rare earth elements in synthetic zircon. Part 2. A single-crystal X-ray study of xenotime substitution. Am Mineral 86:681-689
Finch RJ, Kropf AJ, Hanchar JM (2001b) XAFS spectra of rare earth elements in synthetic zircon. Eleventh Annual V.M. Goldschmidt Conference, Abstr # 3791, LPI Contrib No. 1088, Lunar Planet Inst, Houston (CD-ROM)
Fiske PS, Nellis WJ, Sinha AK (1994) Shock-induced phase transition of $ZrSiO_4$, reversion kinetics, and implications for terrestrial impact craters. EOS, Trans Am Geophys Soc 75:416-417
Fuchs LH, Gebert E (1958) X-ray studies of synthetic coffinite, thorite and uranothorites. Am Mineral 43:243-248

Fukunaga O, Yamaoka S (1979) Phase transformations in ABO_4 type compounds under high pressure. Phys Chem Minerals 5:167-177

Gaines RV, Skinner HCW, Foord EE, Mason B, Rosenzweig A, King VT, Dowty E (1997) Dana's New Mineralogy. Eighth Edition. Wiley and Sons, New York, 1819 p

Gibson GM, Ireland TR (1995) Granulite formation during continental extension in Fiordland, New Zealand. Nature 375:479-482

Glass BP, Liu L, Leavens PB (2002a) Discovery of high-pressure $ZrSiO_4$ polymorph in naturally occurring shock-metamorphosed zircons. Geology 29:371-373

Glass BP, Liu L, Leavens PB (2002b) Reidite: An impact-produced high-pressure polymorph of zircon found in marine sediments. Am Mineral 87:562-565

Goldin BA, Yushkin NP, Fishman MV (1967) A new yttrium mineral, chernovite. Zap Vses Mineral Obshch 96:699-704

Graeser GP, Schwander H, Stalder HA (1973) A solid solution series between xenotime(YPO_4) and chernovite ($YAsO_4$). Mineral Mag 39:145-151

Graeser S, Schwander H (1987) Gasparite-(Ce) and monazite-(Nd): two new minerals to the monazite group. Schweiz Mineral Petrogr Mitt 67:103-113

Hanchar JM (1996) A geochemical investigation of zircon. PhD dissertation, Rensselaer Polytechnic Institute, Troy, New York, 210 p

Hanchar JM, Miller CF, Wooden JL, Bennett VC, Staude J-MG (1994) Evidence from xenoliths for a dynamic lower crust, eastern Mojave desert, California. J Petrol 35:1377-1415

Hanchar JM, Finch RJ, Hoskin PWO, Watson EB, Cherniak DJ, Mariano AN (2001a) Rare earth elements in synthetic zircon: Part 1. Synthesis, and rare earth and phosphorous doping. Am Mineral 86:667-680

Hanchar JM, Finch RJ, Hoskin PWO, Watson EB (2001b) Strain-limited rare-earth element incorporation in zircon. Eleventh Annual V.M. Goldschmidt Conference, Abstract # 3712, LPI Contrib No. 1088, Lunar Planet Inst, Houston (CD-ROM)

Hanchar JM, Finch RJ, Watson EB, Hoskin PWO (2001c) Towards a better understanding of rare earth element partition coefficients in zircon. Proc European Union of Geosciences, XI, Strasbourg, France, April 8-12, 2001, p 677

Hansley PL, Fitzpatrick JJ (1989) Compositional and crystallographic data on REE-bearing coffinite from the Grants uranium region, northwestern New Mexico. Am Mineral 74:263-270

Hawthorne FC, Ferguson RB (1975) Anhydrous sulfates. II. Refinement of the crystal structure of anhydrite. Can Mineral 13:289-292

Hazen RM, Finger LW (1979) Crystal structure and compressibility of zircon at high pressure. Am Mineral 64:196-201

Hazen RM, Mariathasan JWE (1982) Bismuth vanadate: A high-pressure, high-temperature crystallographic study of the ferroelastic-paraelastic transition. Science 216:991-993

Herzenberg R (1946) Nuevos minerales de Bolivia. Bol. Técnio No 1, Fac Nac Ingeneria, Univ Técnica Oruro (1946)

Hinton RW, Upton BGJ (1991) The chemistry of zircon: Variations within and between large crystals from syenite and alkali basalt xenoliths. Geochim Cosmochim Acta 55:3287-3302

Hinton RW, MacDonald R, McGarvie DW, Tindle A, Harley SL (2003) The possible role of hydrogen in the substitution of rare earth elements into zircon. Spring AGU-EUG-EGS Joint Assembly, Nice, France, April 6-11, 2003, Geophysical Research Abstracts 5 05968

Hirano M, Morikawa H, Inagaki M, Toyoda M (2002a) Direct synthesis of new zircon-type $ZrGeO_4$ and $Zr(Ge,Si)O_4$ solid solutions. J Am Ceram Soc 85:1915-1920

Hirano Y, Guedes I, Grimsdith M, Loong C-K, Wakabayashi N, Boatner LA (2002b) Brillouin-scattering study of the elastic constants of $ErVO_4$. J Am Ceram Soc 85:1001-1003

Hoekstra HR, Fuchs LH (1956) Synthesis of coffinite-$USiO_4$. Science 123:105

Hoskin PWO (2000) Patterns of chaos: fractal statistics and the oscillatory chemistry of zircon. Geochim Cosmochim Acta 64:1905-1923

Hoskin PWO, Rodgers KA (1996) Raman spectral shift in the isomorphous series $(Zr_{1-x}Hf_x)SiO_4$. Eur J Sol State Inorg Chem 33:1111-1121

Hoskin PWO, Kinny PD, Wyborn D, Chappel BW (2000) Identifying accessory mineral saturation during differentiation in granitoid magmas: an integrated approach. J Petrol 41:1365-1396

Janeczek J (1991) Composition and origin of coffinite from Jachymov, Czechoslovakia. Neues Jahrb Mineral Monatsh 9:385-395

Janeczek J, Ewing RC (1992) Dissolution and alteration of uraninite under reducing conditions. J Nucl Mater 190:157-173

Janeczek J, Ewing RC (1996) Phosphatian coffinite with rare earth elements and Ce-rich françoisite-(Nd) from sandstone beneath a natural fission reactor at Bangombé, Gabon. Mineral Mag 60:665-669

Jayaraman A, Kourouklis GA, Espinoza GP, Cooper SA, Van Uitert LG (1987) A high-pressure Raman study of

yttrium vanadate (YVO_4) and the pressure-induced transition from the zircon-type to the scheelite-type structure. J Phys Chem Solids 48:755-759

Kazei ZA, Kolmakova NP (1995) Magnetoelastic anomalies in the thermal expansion of rare-earth vanadates RVO_4. Sov Phys Solid State 37:577-582

Knittle E (1995) Static compression measurements of equations of state. *In* Mineral Physics and Crystallography. A Handbook of Physical Constants. AGU Reference Shelf, Ahrens TJ (ed) American Geophysical Union, Washington, DC, 2:8-142

Knittle E, Williams Q (1993) High-pressure Raman spectroscopy of $ZrSiO_4$: Observation of the zircon to scheelite transition at 300 K. Am Mineral 78:245-252

Kusaba K, Syono Y, Kikuchi M, Fukuoka K (1985) Shock behavior of zircon: phase transition to scheelite structure and decomposition. Earth Planet Sci Lett 72:433-439

Kusaba K, Takehiko Y, Masae K, Yasuhiko S (1986) Structural considerations on the mechanism of the shock-induced zircon-scheelite transition in $ZrSiO_4$. J Phys Chem Solids 47:675-679

Leroux H, Reimold WU, Koeberl C, Hornemann U, Doukhan, J-C (1999) Experimental shock deformation in zircon: a transmission electron microscopic study. Earth Planet Sci Lett 169:291-301

Liu L (1979) High-pressure phase transformations in baddeleyite and zircon, with geophysical implications. Earth Planet Sci Lett 44:390-396

Lohmüller G, Schmidt G, Deppisch B, Gramlich V, Scheringer C (1973) Die Kristallstrukturen von Yttrium-Vanadat, Lutetium-Phosphat und Lutetium-Arsenat. Acta Crystallogr B29:141-142

Lunga S (1966) Etude des courbes de liquidus et des proprieties thermodynamiques des systems SiO_2-ThO_2 et SiO_2-ThO_2-UO_2. J Nucl Mater 19:157-159

Maas R, Kinny PD, Williams IS, Froude DO, Compston W (1992) The Earth's oldest known crust: a geochronological and geochemical study of 3900-4200 Ma old detrital zircons from Mt. Narryer and Jack Hills, Western Australia. Geochim Cosmochim Acta 56:1281-1300

Mariathasan JWE, Hazen RM, Finger LW (1986) Crystal structure of the high-pressure form of $BiVO_4$. Phase Trans 6:165-174

Mazhenov NA, Nurgaliev BZ, Muldakhmetov KZ (1988) Scheelite modification of neodymium arsenate. Izv Akad Nauk SSSR, Neorg Mater 24:1163-1165 (English translation in Inorg Mater 24:991-993)

Melcher RL (1976) The anomalous elastic properties of materials undergoing cooperative Jahn-Teller phase transitions. *In* Physical Acouostics. Mason WP, Thurston RN (eds) Academic Press, New York, p 1-77

Mereiter K, Preisinger A (1986) Kristalstrukturdaten der Wismutminerale Atelestit, Mixit und Pucherit. Anz Oesterr Akad Wiss math-naturwiss Klass 123:79-81

Miles NM, Hogarth DD, Russel DS (1971) Wakefieldite, yttrium vanadate, a new mineral from Quebec. Am Mineral 56:395-410

Mooney RC (1948) Crystal structure of tetragonal bismuth arsenate, $BiAsO_4$. Acta Crystallogr 1:163-165

Mrose ME, Rose JH, Jr (1961) Behierite, $(Ta,Nb)BO_4$, a new mineral from Manajaka, Madagascar. Geol Soc Am Abstracts 1961 Ann Meetings, p 111A; abstracted by Fleischer M (1962) New mineral names. Am Mineral 47:414

Mumpton FA, Roy R (1961) Hydrothermal stability studies of the zircon-thorite group. Geochim Cosmochim Acta 21:217-238

Mursic Z, Vogt T, Frey F (1992) High-temperature neutron powder diffraction study of $ZrSiO_4$ up to 1,900 K. Acta Crystallogr B 48:584-590

Ni Y, Hughes JM, Mariano AN (1995) Crystal chemistry of the monazite and xenotime structures. Am Mineral 80:21-26

Nipko JC, Loong C-K, Kern S, Abraham MM, Boatner LA (1997) Crystal field splitting and anomalous thermal expansion in $YbVO_4$. J Alloys Comp 250:569-572

Nyman H, Hyde BG, Andersson S (1984). Zircon, anhydrite, scheelite and some related structures containing bisdisphenoids. Acta Crystallogr B 40:441-447

Oka Y, Yao T, Yamamoto N (2000) Hydrothermal synthesis and crystal structures of zircon-type $LaVO_4$ and a new compound LaV_3O_9. J Solid State Chem 152:486-491

Plant JA, Simpson PR, Smith B, Windley BF (1999) Uranium ore deposits: Products of the radioactive Earth. Rev Mineral 38:255-319

Qurashi MM, Barnes WH (1952) A preliminary structure for pucherite, $BiVO_4$. Am Mineral 37:423-426

Qurashi MM, Barnes WH (1953) The structure of pucherite, $BiVO_4$. Am Mineral 38:489-500

Ramakrishnan SS, Gokhale KVGK, Subarrao EC (1969) Solid solubility in the system zircon-hafnon. Mater Res Bull 4:323-328

Range K-J, Meister H (1990). $ErVO_4$-II, a scheelite-type high-pressure modification of erbium orthovanadate. Acta Crystallogr C 46:1093-1094

Reid AF, Ringwood AE (1969) Newly observed high pressure transformations in Mn_3O_4, $CaAl_2O_4$, and $ZrSiO_4$. Earth Planet Sci Lett 6:205-208

Rice CE, Robinson WR (1976) Lanthanum orthovandate. Acta Crystallogr B 32:2232-2233
Ríos S, Malcherek T, Salje EKH, Domeneghetti C (2000) Localized defects in radiation-damaged zircon. Acta Crystallogr B 56:947-952
Robinson K, Gibbs GV, Ribbe PH (1971) The structure of zircon: a comparison with garnet. Am Mineral 56:782-790
Rudnick RL, Fountain DM (1995) Nature and composition of the continental crust: a lower crustal perspective. Rev Geophys 33:267-309
Sandercock JR, Palmer SB, Elliot RJ, Hayes W, Smith SRP, Young AP (1972) Brillouin scattering, ultrasonic and theoretical studies of acoustic anomalies in crystals showing Jahn-Teller phase transitions. J Phys C: Solid State Phys 5:3126-3146
Schwarz VH (1963) Die phosphate, arsenate und vanadate der Seltenen erden. Z Anorg Allg Chemie 323:44-56
Scott HP, Williams Q, Knittle E (2002) Ultralow compressibility silicate without highly coordinated silicon. Phys Rev Lett 88:015506-1-015506-4
Sejkora, Rídkošil (1994) Tetrarooseveltite, ß-Bi(AsO_4), a new mineral species from Moldava deposit, the Krušné hory Mts., Northwestern Bohemia, Czech Republic. Neues Jahrb Mineral Monatsh 1994:179-184
Shannon RD (1976) Revised effective ionic radii and systematic studies of interatomic distances in halides and chalcogenides. Acta Crystallogr A 32:751-767
Skanthakumar S, Loong C-K, Soderholm L, Nipko J, Richardson JW, Abraham MM, Boatner LA (1995) Anomalous temperature dependence of the lattice parameters in $HoPO_4$ and $HoVO_4$: Rare earth quadrapolar effects. J Alloys Comp 225:595-598
Solar GS, Pressley RA, Brown M, Tucker RD (1998) Granite ascent in convergent orogenic belts: Testing a model. Geology 26:711-714
Speer JA (1982a) Zircon. Rev Mineral 5:67-112
Speer JA (1982b) The actinide orthosilicates. Rev Mineral 5:113-135
Speer JA, Cooper BN (1982) Crystal structure of synthetic hafnon, $HfSiO_4$, comparison with zircon and the actinide orthosilicates. Am Mineral 67:804-808
Stubican V-S, Roy R (1963) High-pressure scheelite-structure polymorphs of rare-earth vanadates and arsenates. Z Kristallogr 119:90-97
Subbarao EC, Agrawal DK, McKinstry HA, Sallese CW, Roy R (1990) Thermal expansion of compounds of zircon structure. J Am Ceram Soc 73:1246-1252
Taylor M, Ewing RC (1978) The crystal structures of the $ThSiO_4$ polymorphs: huttonite and thorite. Acta Crystallogr B 34:1074-1079
Taylor SR, McLennan SM (1995) The geochemical evolution of the continental crust. Rev Geophys 33:241-265
Tomaschek F, Ballhaus C (2003) Zircon-xenotime solid-solubility: An experimental study. Spring AGU-EUG-EGS Joint Assembly, Nice, France, April 6-11, 2003, Geophys Res Abstr 5:13283
van Westrenen W, Wood BJ, Blundy JD (2001) A predictive thermodynamic model of garnet-melt trace element partitioning. Contrib Mineral Petrol 142:219-234
van Westrenen W, Frank MR, Hanchar JM, Fei Y, Finch RJ, Zha C-S (2003a) *In situ* determination of the compressibility of synthetic pure zircon ($ZrSiO_4$) and the onset of the zircon-reidite phase transition. Am Mineral 88 (accepted)
van Westrenen W, Frank MR, Fei Y, Hanchar JM, Finch RJ, Zha C-S (2003b) *In situ* measurements of the compressibility of pure and trace element doped synthetic zircon. Spring AGU-EUG-EGS Joint Assembly, Nice, France, April 6-11, 2003 (abstr)
Vegard L (1916) Results of crystal analysis. Philos Mag Ser 6, 32:65-96
Vegard L (1926) Results of crystal analysis. Philos Mag Ser 7, 1:1151-1193
Vervoort JD, Patchett PJ, Gehrels GE, Nutman AP (1996) Constraints on early Earth differentiation from hafnium and neodymium isotopes. Nature 379:624-627
Weaver BL, Tarney J (1984) Major and trace element composition of the continental lithosphere. *In* Structure and Evolution of the Continental Lithosphere. Physics and Chemistry of the Earth, Pollack HN, Murthy VR (eds) Pergamon Press, Oxford, 15:39-68
Weber G, Range K-J (1996) Die Kristallstruktur von Calziumchromate(VI), $CaCrO_4$. Z Naturforsch 51B:751-753
Wedepohl KH (1995) The composition of the continental crust. Geochim Cosmochim Acta. 59:1217-1232
Wilde SA, Valley JW, Peck WH, Graham CM (2001) Evidence from detrital zircons for the existence of continental crust and oceans on the Earth 4.4 Gyr ago. Nature 409:175-178
Williford RE, Weber WJ, Devanathan R, Cormak AN (1999) Native vacancy migrations in zircon. J Nucl Mater 273:164-170
Williford RE, Begg BD, Weber WJ, Hess NJ (2000) Computer simulation of Pu^{3+} and Pu^{4+} substitutions in zircon. J Nucl Mater 278:207-211